AGU PUBLICATIONS

JGR

Journal of Geophysical Research: Oceans

RESEARCH ARTICLE

10.1002/2016JC012059

Wind modulation of upwelling at the shelf-break front off Patagonia: Observational evidence

M. M. Carranza[1], S. T. Gille[1], A. R. Piola[2,3,4], M. Charo[2], and S. I. Romero[2,3]

[1]Scripps Institution of Oceanography, University of California San Diego, La Jolla, California, USA, [2]Departamento Oceanografía, Servicio de Hidrografía Naval, Buenos Aires, Argentina, [3]Departamento Ciencias de la Atmósfera y los Océanos, Facultad de Ciencias Exactas y Naturales, Universidad de Buenos Aires, Argentina and Instituto Franco-Argentino sobre Estudios de Clima y sus Impactos, CNRS/CONICET, Buenos Aires, Argentina, [4]Consejo Nacional de Investigaciones Científicas y Técnicas, Buenos Aires, Argentina

Key Points:
- Satellite Chl-a composites segregated by wind direction suggest that along-front winds modulate shelf-break upwelling
- In situ hydrographic observations show isopycnal tilting and changes in stratification that are consistent with Ekman dynamics
- Subsurface Chl-a fluorescence provides further evidence of the influence of along-front winds on Chl-a concentrations at the front

Correspondence to:
M. M. Carranza,
maucarranza@ucsd.edu

Citation:
Carranza, M. M., S. T. Gille, A. R. Piola, M. Charo, and S. I. Romero (2017), Wind modulation of upwelling at the shelf-break front off Patagonia: Observational evidence, *J. Geophys. Res. Oceans*, *122*, 2401–2421, doi:10.1002/2016JC012059.

Received 15 JUN 2016
Accepted 12 FEB 2017
Accepted article online 15 FEB 2017
Published online 24 MAR 2017

Abstract The South-Atlantic Patagonian shelf is the largest chlorophyll-a (Chl-a) hot spot in Southern Ocean color images. While a persistent 1500 km long band of high Chl-a along the shelf-break front (SBF) is indicative of upwelling, the mechanisms that drive it are not entirely known. Along-front wind oscillations can enhance upwelling and provide a nutrient pumping mechanism at shelf-break fronts of western boundary currents. Here we assess wind-induced upwelling at the SBF off Patagonia from daily satellite Chl-a and winds, historical hydrographic observations, cross-shelf Chl-a fluorescence transects from two cruises, and in situ winds and water column structure from a mooring site. Satellite Chl-a composites segregated by along-front wind direction indicate that surface Chl-a is enhanced at the SBF with southerly winds and suppressed with northerly winds. Northerly winds also result in enhanced Chl-a further offshore (~25–50 km). Synoptic transects as well as mean hydrographic sections segregated by along-front winds show isopycnals tilted upward for southerly winds. Spring observations from the mooring also suggest that southerly winds destratify the water column and northerly winds restratify, in agreement with Ekman transport interacting with the front. Moreover, changes in water column temperature lag along-front wind forcing by 2–4 days. Our results suggest that oscillations in along-front winds, on timescales typical of atmospheric storms (2–10 days), can significantly modulate the upwelling and Chl-a concentrations at the SBF off Patagonia, revealing the importance of wind-induced upwelling for shelf-slope exchange at shelf-break fronts of western boundary currents.

1. Introduction

Continental shelves support high primary productivity and are responsible for more than 40% of the carbon sequestration of the world's ocean [e.g., *Muller-Karger*, 2005]. The Patagonian shelf, characterized by a western-boundary current regime along the eastern coastline of South America from about 38°S to 55°S, stands out as a hot spot in satellite chlorophyll-a (Chl-a), indicative of phytoplankton abundance, with typical Chl-a concentrations an order of magnitude larger than those found in the open ocean. Rates of primary production are comparable to those found in the most productive regions (e.g., eastern boundary upwelling systems [*Carr and Kearns*, 2003; *Garcia et al*., 2008; *Chavez and Messié*, 2009; *Lutz et al*., 2010; *Segura et al*., 2013]), which sustain abundant marine life at higher trophic levels [*Acha et al*., 2004; *Bogazzi et al*., 2005; *Campagna et al*., 2006; *Falabella*, 2009] and the largest marine ecosystem of the Southern Hemisphere [*Bisbal*, 1995; *Longhurst*, 2007; *Heileman*, 2009]. Large diatom blooms [*Garcia et al*., 2008; *Carreto et al*., 2016] are responsible for substantial rates of absorption of atmospheric CO_2 [*Schloss et al*., 2007], making the region one of the strongest CO_2 sinks per unit area of the world's ocean [*Bianchi*, 2005; *Bianchi et al*., 2009; *Arruda et al*., 2015].

A prominent narrow band of high satellite Chl-a along the shelf break closely follows the 200 m isobath (see Figure 1) and is persistent in climatological means [e.g., *Acha et al*., 2004; *Saraceno et al*., 2005; *Rivas*, 2006; *Romero et al*., 2006; *Signorini et al*., 2006]. Such persistent enhancement of Chl-a at the shelf break is indicative of upwelling of nutrient-rich waters, but the mechanisms that drive such upwelling are still under debate (see section 2). Regardless of the mechanism behind the formation and maintenance of the strong upwelling at the shelf-break front (SBF) off Patagonia, winds have the potential to interact with the frontal

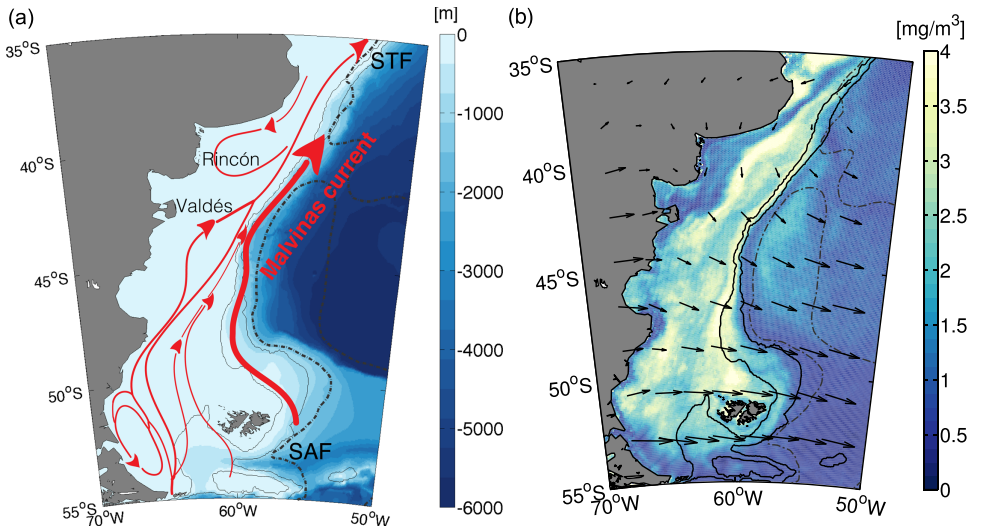

Figure 1. (a) Bathymetry of the Patagonian shelf from GEBCO with schematic of mean circulation, adapted from *Piola and Falabella* [2009]. (b) Satellite Chl-a amplitude (annual maximum-annual minimum) based on monthly means for the period 2000–2011, with mean summer wind vectors overlaid. Solid black contours indicate the 200 and 1000 m isobaths. The Sub-Antarctic Front (SAF) and Sub-Tropical Front (STF) from *Orsi et al.* [1995] are shown by dashed black lines.

circulation and modulate the nutrient supply to the euphotic zone, decouple biological trophic interactions, and, thus, impact phytoplankton growth and Chl-a concentrations [e.g., *Franks and Walstad*, 1997; *Nagai et al.*, 2008; *Siedlecki et al.*, 2011]. The scope of this paper is to explore wind-related physical forcing on atmospheric synoptic timescales as a possible driver of Chl-a variability at the SBF off Patagonia, leveraging existing observations in the region.

On scales of atmospheric synoptic storms (>500 km, 2–10 days), wind can modify the upwelling at a front by several means: (1) direct wind-driven vertical mixing [e.g., *Klein and Hua*, 1988; *Nagai et al.*, 2006, 2008], (2) variable wind stress relative to the surface current to either side of the jet that induces Ekman pumping/suction [e.g., *Lee et al.*, 1994; *Zhang et al.*, 2011], and/or (3) along-front oscillations in the wind interacting with the frontal structure (i.e., sloping isopycnals) through Ekman transport [*Siedlecki et al.*, 2011]. While the former is primarily associated with wind intensity, the two latter are intrinsically linked to wind directionality relative to the front and their interaction through Ekman dynamics. Previous studies on wind-front interactions on synoptic timescales have largely focused on open-ocean fronts or the Middle Atlantic Bight (MAB) coastal system, with physical attributes similar to the Patagonian shelf-break region (i.e., western boundary current system) but also major differences (see section 2 and *Matano and Palma* [2008]). This study represents the first attempt to look for evidence of synoptic-scale wind-induced upwelling at the Patagonian SBF. The three mechanisms will be considered and are introduced below based on previous work.

Enhanced wind-driven mixing can increase nutrient concentrations in the mixed layer through mixed-layer depth deepening and entrainment [*Klein and Coste*, 1984], particularly near fronts [*Klein and Hua*, 1988]. Modeling studies also show that vertical mixing alone can enhance fine-scale upwelling along isopycnals on the less dense side of fronts, due to the development of secondary vertical circulations that are driven by mixing [*Nagai et al.*, 2006, 2008]. Thus, high winds can potentially enhance surface Chl-a concentrations, particularly in summer [e.g., *Swart et al.*, 2015; *Carranza and Gille*, 2015], when strong stratification develops and wind-driven mixing can episodically entrain Chl-a and/or nutrient-rich subsurface waters into the mixed layer. Although we cannot rule out this mechanism, correlations between daily wind speed and Chl-a anomalies are generally small and show relative minima at the SBF off Patagonia [see *Carranza and Gille*, 2015, Figure 7a], suggesting that direct wind-driven vertical mixing has little influence on the Chl-a response at this SBF.

Wind directionality can also modify upwelling rates and nutrient pumping near fronts. Wind direction may interact with the frontal circulation and modulate the location and intensity of the upwelling at open ocean fronts, with consequences for phytoplankton accumulation and production [*Franks and Walstad*, 1997;

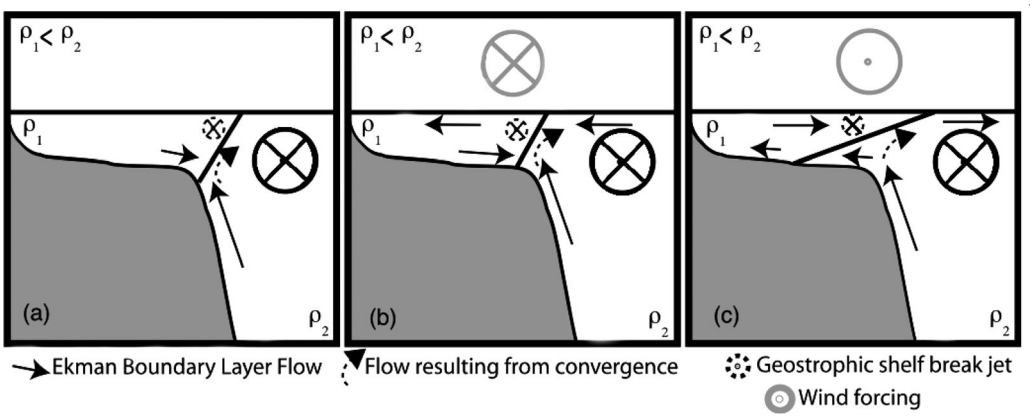

Figure 2. Schematic diagram showing the effect of along-front winds on the upwelling at a shelf-break front, adapted for the Southern Hemisphere and modified from *Siedlecki et al.* [2011]. In their model, alongshore variations (i.e., frontal meandering and eddies) are neglected. Frontal structure with (a) no wind forcing, (b) southerly winds, and (c) northerly winds. Southerly winds lead to Ekman transport in the surface layer onshore, steepening frontal isopycnals and enhancing the upwelling at the shelf break, whereas northerly winds lead to offshore Ekman transport, flattening isopycnals and suppressing upwelling at the SBF. Note that for the no-wind scenario, the presence of a slope jet with strong shear in their model produces a reversal of the flow at depth over the slope and, hence, convergence in the BBL. The role of this process in the Patagonian SBF is questionable due to the presence of a strong slope current, and the dominant mechanism at play is uncertain [see, e.g., *Matano and Palma*, 2008]. Nonetheless, upwelling is expected to occur at the SBF off Patagonia in the no-wind case as well, and we kept the arrows as in the original schematic.

Nagai et al., 2008; *Whitt et al.,* 2017]. Theoretical and numerical studies supported by observations have shown that along-front winds can substantially modify the vertical circulation through Ekman dynamics [e.g., *Lee et al.*, 1994; *Thompson*, 2000; *Thomas and Lee*, 2005]. In particular, downfront winds (i.e., in the direction of the frontal jet), by advecting surface waters in the Ekman layer from the dense to the less dense side of a front, can enhance frontogenesis as a consequence of wind-driven gravitational instabilities and nonlinear Ekman pumping, modifying stratification and upwelling/subduction rates in mesoscale oceanic fronts [*Thomas and Lee*, 2005; *Thomas and Ferrari*, 2008].

In the vicinity of a frontal jet, enhanced upwelling may be caused by along-front wind stress variations in the cross-front direction induced by changes in the magnitude of surface currents, which can modify the effective wind stress [e.g., *Lee et al.*, 1994; *Zhang et al.*, 2011; *Hutchinson et al.*, 2010; *McGillicuddy*, 2016]. Even under uniform wind forcing, the differential along-front wind stress to either side of the front can produce Ekman transport divergences/convergences and upwelling/downwelling through Ekman suction/pumping (i.e., due to the jet-induced wind-stress curl). As will be further discussed, under the assumption that synoptic winds are spatially uniform over the scale of the front, and stronger in magnitude than oceanic currents, such a mechanism would consistently intensify the upwelling onshore of the Malvinas Current jet (see Figure 1), regardless of along-front wind orientation (i.e., up or downfront winds).

At shelf-break fronts of western boundary currents, oscillations in the along-front component of the winds can also modulate the upwelling, providing a mechanism for transient nutrient supply to the euphotic zone [*Houghton et al.*, 1988; *Fratantoni and Pickart*, 2003; *Siedlecki et al.*, 2011], with stronger oscillating winds of longer periods resulting in higher biological production. Based on a numerical model configured for the MAB, *Siedlecki et al.* [2011] suggest that when wind oscillations are aligned with a shelf-break front, Ekman transport in the surface layer can tilt the isopycnals associated with the front, changing cross-front circulation patterns and frontal upwelling. At a SBF that separates less dense shelf waters from denser open ocean waters and in the absence of alongshore pressure gradients, upfront winds are expected to flatten isopycnals, producing upwelling of nutrient-rich waters in the Bottom Boundary Layer (BBL) from the slope onto the shelf (i.e., onwelling [see *Siedlecki et al.*, 2011]. The reversal of the winds (i.e., downfront winds), by steepening isopycnals, provides a mechanism for nutrient pumping to the euphotic layer, with potential consequences for primary production. For the Patagonian shelf configuration, upwelling at the SBF would be favored by southerly winds (i.e., from the south or downfront) associated with onshore Ekman transport in the surface layer, and more vertical isopycnals. In contrast, northerly winds (i.e., from the north or upfront) with associated Ekman transport offshore tend to restratify and flatten isopycnals at the front (see schematic in Figure 2, adapted for the Southern Hemisphere from *Siedlecki et al.* [2011]).

Although winds in the Patagonia region are not predominantly upwelling favorable or downfront with respect to the Malvinas Current flow (i.e., the western boundary current), synoptic weather can produce wind patterns that substantially deviate from the prevailing westerly mean wind fields [*Jones and Simmonds*, 1993; *Vera*, 2003; *Eichler and Gottschalck*, 2013], and variability in the along-shelf component of the winds can potentially modulate the upwelling and productivity of the SBF off Patagonia.

This study takes advantage of satellite data and existing in situ observations in the region to evaluate the hypothesized wind-induced upwelling mechanism associated with along-front wind oscillations and the interaction with frontal isopycnals [*Siedlecki et al*., 2011], although upwelling due to differential wind stress under uniform wind forcing is also discussed. We use high-resolution satellite observations of winds and ocean color as well as hydrography and in situ Chl-a fluorescence measurements from cruises and a mooring site to assess whether along-front winds modulate the upwelling at the SBF off Patagonia. We explore to what extent these upwelling patterns modulate biological productivity, addressing the biological impact of the oscillating wind effect on the upwelling through the Chl-a response. Section 2 describes general characteristics of the Patagonian shelf region and proposed mechanisms for the local upwelling at the shelf break. In section 3 we present the data sources used. Satellite-based results suggest that along-front winds can modulate Chl-a at the SBF, potentially through isopycnal tilting, and are presented in section 4.1. We show synoptic evidence of isopycnal tilting under opposing along-front wind conditions from hydrographic sections across the SBF (section 4.2), as well as composite sections from historical hydrographic stations segregated by wind direction (section 4.3). Further evidence of wind-driven upwelling from a SBF mooring site that acquired meteorological and water column hydrographic data is presented in section 4.4. Results are further discussed in section 5, and conclusions follow in section 6.

2. Background: General Characteristics of the Patagonian Shelf and Physical Mechanisms for Shelf-Break Upwelling

The Patagonian shelf spans over 1.2 million km^2 of ocean and is under the influence of predominantly westerly winds and high tidal energy [e.g., *Palma et al*., 2004]. The circulation over the shelf is characterized by wind-driven northeastward flow of low-salinity waters that outflow from the Strait of Magellan [*Guerrero and Piola*, 1997; *Palma et al*., 2004]. The shelf is bounded on the east by the northward flowing Malvinas Current (i.e., slope western boundary current, see Figure 1a) which supplies cold nutrient-rich subantarctic waters to the shelf [*Piola et al*., 2010; *Painter et al*., 2010]. On the shelf's outer edge, the 1500 km long SBF separates the Malvinas Current ($T < 15$ °C, $S_p \sim 34.2$ psu [e.g., *Valla and Piola*, 2015]) from seasonally warmer and relatively fresher shelf waters ($S_p < 33.9$ psu [e.g., *Guerrero and Piola*, 1997; *Palma et al*., 2008]). The transition between shelf and open ocean waters is therefore characterized by moderate cross-front temperature and salinity gradients [*Romero et al*., 2006; *Painter et al*., 2010; *Valla and Piola*, 2015]. Observations show that the shelf-break salinity front, which closely follows the 33.9 psu isohaline [*Piola et al*., 2010; *Painter et al*., 2010], is associated with nitrate maxima, located at or inshore of the surface temperature minimum and density maximum [*Romero et al*., 2006; *Painter et al*., 2010; *Poulton et al*., 2013; *Valla and Piola*, 2015]. The seasonal variability in light intensity and nutrient supply to the mixed layer associated with changes in stratification control the strong variability of phytoplankton abundance [*Signorini et al*., 2006]. Though nutrient observations are scarce, recent adjoint sensitivity experiments suggest that phytoplankton productivity is limited by macronutrients (i.e., nitrate) over the shelf, whereas in the outer shelf, productivity is presumably iron limited [*Song et al*., 2016]. Bottom shelf water, presumably rich in iron, could also be a source of iron to the outer shelf [*Siedlecki et al*., 2012]. Therefore, the exchange of water masses across the SBF impacts biological productivity [e.g., *Piola et al*., 2010; *Brink*, 2016]. However, the underlying mechanisms that regulate the cross-shelf exchange between the open ocean and shelf waters in this region are not well known.

Shelf-break upwelling can be generated by internal processes associated with the convergence and detachment of the BBL over shelves dominated by cyclonic currents [e.g., *Gawarkiewicz and Chapman*, 1992; *Chapman and Lentz*, 1994; *Chapman*, 2002]. However, BBL detachment cannot fully explain the strong upwelling inferred from observations at the SBF off Patagonia [*Matano and Palma*, 2008; *Miller et al*., 2011]. In situ and remote sensing observations suggest that intense shelf-break upwelling can reach 13–29 m d^{-1} [*Valla and Piola*, 2015], while average modeled upwelling rates are 8 m d^{-1} [*Matano and Palma*, 2008; *Combes and Matano*, 2014]. Using numerical experiments based on idealized conditions for the Patagonian shelf,

Matano and Palma [2008] showed that, in the absence of an externally imposed horizontal density gradient and the presence of a strong slope current flowing in the direction of coastally trapped waves (i.e., Malvinas Current), the magnitude of upwelling generated by the detachment of the BBL is very small (i.e., $\sim$0.2 m d^{-1}). Instead, they found that the upwelling at the SBF off Patagonia is mainly driven by horizontal flow divergences due to the spreading of the western boundary current onto the shelf, and the magnitude of the upwelling is proportional to the slope current transport. The shelf-break upwelling mechanism proposed by *Matano and Palma* [2008] is controlled by the along-shelf pressure gradient, which drives downstream divergences of the slope current. Their theory is supported by analytical solutions of the simplified shallow-water equations [e.g., *Miller et al*., 2011], as well as by higher-resolution modeling experiments with realistic bathymetry and forcing [*Combes and Matano*, 2014]. In situ surface current observations are sparse in the region, and the magnitude of such process remains to be tested with observations.

Although, in the northern sector of the Patagonian continental slope, observations show zonal displacements of the Malvinas current flow and baroclinic jets that are responsible for slope water intrusions to the shelf [*Carreto et al*., 1995; *Franco et al*., 2008; *Piola et al*., 2010, 2013], the steady northward flow is mostly barotropic and strongly controlled by bottom topography [*Vivier and Provost*, 1999; *Piola et al*., 2010, 2013]. In the absence of alongshore variations (i.e., frontal meandering and eddies), along-front oscillating winds may produce net upward pumping of nutrients at the shelf break on subseasonal timescales (i.e., $<$15 days) [*Siedlecki et al*., 2011].

Previous studies that have looked into wind-driven physical controls of satellite Chl-a in the Patagonian shelf region have focused on seasonal to interannual timescales or have analyzed case studies, often based on in situ observations and models [e.g., *Saraceno et al*., 2005; *Garcia et al*., 2008; *Signorini et al*., 2009; *Machado et al*., 2013]. *Saraceno et al*. [2005] discussed satellite Chl-a variability at the SBF in relation to meridional winds in the context of interannual variability of spring blooms; years with stronger northerly winds were associated with higher Chl-a concentrations than years when northerly winds were moderate or from the south. They suggested that eastward Ekman transport could result in the interleaving of the different water masses at the SBF and enhance vertical stability, retaining phytoplankton in the euphotic zone [*Podestá*, 1990]. Coastally trapped waves, generated by remote wind forcing, were also suggested as a possible mechanism that could explain 70 day fluctuations in SST and Chl-a 8 day fields [*Saraceno et al*., 2005], in agreement with previous studies of the variations of the intensity of the western boundary current [*Vivier and Provost*, 1999; *Vivier et al*., 2001]. The modulation of the upwelling at the SBF off Patagonia by the winds, on subseasonal timescales shorter than 15 days, which is the focus of our study, has not been previously addressed from observations.

3. Data and Methods

3.1. Satellite Data

We use satellite winds and Chl-a estimates to evaluate the influence of along-front winds on phytoplankton blooms near the SBF off the eastern coast of Patagonia. The long satellite records (i.e., 12 years) allow us to assess statistical significance and complement evidence of wind-induced upwelling at the SBF from in situ observations.

Daily satellite Chl-a serves as a proxy for phytoplankton biomass within one optical depth of the surface (e.g., *Morel and Berthon,* 1989). The data are available at 9 km resolution, covering the period 2000–2011 for which satellite wind data are also available. We use satellite Chl-a derived using the Southern Ocean SPGANT algorithm [*Mitchell and Kahru*, 2009], which uses the maximum band-ratio algorithm [*O'Reilly et al*., 1998], but with coefficients fitted to Southern Ocean data, and which merges satellite data from several sensors (i.e., OCTS, SeaWiFS, MODIS-Aqua, and VIIRS). Although SPGANT has not been validated against in situ Chl-a for this particular region, our conclusions do not rely on Chl-a absolute values and are not sensitive to the choice of the Chl-a data set used (e.g., Chl-a from GlobColour leads to qualitatively similar results). Because Chl-a is lognormally distributed, for averaging we use a geometric mean, obtained by averaging the logarithm of Chl-a and then inverse-transforming the averaged logarithm [*IOCCG*, 2004].

We use Cross-calibrated Multi-Platform (CCMP) 6 hourly winds for the period 2000–2011 [*Atlas et al*., 2011]. CCMP winds result from a 4-D variational analysis based on multiple satellite data sets, in situ winds and European Centre for Medium-Range Weather Forecasts (ECMWF) analysis winds. Data gaps in CCMP winds

Table 1. Summary of In Situ Observations Presented in This Study[a]

Data Type	Location	Time Period	Wind Direction
GEF-1 Transect (Rincón)	~41°S, 57°W	10 Oct 2005	Northerly
GEF-1 Transect (Valdés)	~44°S, 60°W	13–15 Oct 2005	Southerly
GEF-3 Transect (Rincón)	~41°S, 57°W	23–25 Oct 2006	Southerly
GEF mooring	~44°S, 60°W	16 Oct to 5 Dec 2006	Variable
		1988–1989	
Historical hydrography (SHN and INIDEP)	See Figure 7a	1992–1995, 1997–1998, 2003, 2005, 2006	Variable

[a]Web links for data sources can be found in the data section and acknowledgements.

are expected, since satellite wind measurements are affected by rain [*Atlas et al*., 2011]. CCMP winds are preferred over single-scatterometer winds because they capture the high-frequency variability in the winds and show coherence with high-resolution in situ winds from meteorological buoys up to the diurnal scale [*Carranza and Gille*, 2015]. In addition, unlike single-scatterometer winds, CCMP winds show no directional bias against in situ observations from buoys. Both microwave radiometers and scatterometer measurements are more closely related to wind stress (i.e., momentum relative to the ocean) than to the actual wind [*Atlas et al*., 2011], but are reported as 10 m equivalent neutral wind speed for calibration purposes. The conversion of stress to wind speed at 10 m height considers influences of atmospheric stability [*Bourassa et al*., 2010]; however, equivalent neutral winds are also relative to currents [*Kelly et al*., 2001; *Chelton*, 2004]. For this analysis, 25 km resolution winds were linearly interpolated into the 9 km grid of the Chl-a data.

The 9 km resolution of the satellite data resolves frontal variability over spatial scales greater than 18 km. This is sufficient considering that the frontal region (i.e., the horizontal scale over which isopycnals slope upward) from theoretical considerations scales approximately as twice the Rossby radius of deformation [*Franks*, 1992], which gives R ~ 10–15 km for a density contrast between shelf and slope water masses of ~0.8–1 kg m^{-3}, a total water column depth of 200 m, and a range of latitudes between ~38°S and 50°S characteristic of the Patagonian SBF.

3.2. In Situ Observations

We extend the analysis from satellite fields to examine processes occurring throughout the water column in the vicinity of the SBF using the historical database of hydrographic stations collected in the region by the Servicio de Hidrografía Naval (SHN, www.hidro.gov.ar/ceado/ceado.asp) and the Instituto Nacional de Investigación y Desarrollo Pesquero (INIDEP, http://www.inidep.edu.ar/oceanografia/) in Argentina. A summary of all in situ observations used in this study is presented in Table 1.

3.2.1. Historical Hydrographic Stations

We examined the historical database of hydrographic stations from the SHN from 1987 onward, when CCMP satellite winds are available, as well as stations collected by INIDEP for the years 1992–1998. For this study, we analyzed stations within 200 km of the 200 m isobath, between approximately 38°S and 50°S. We restricted the analyses to stations south of 38°S to avoid buoyancy effects from the La Plata River plume, which outflows anticyclonically toward the north near 36°S, and may hinder isopycnal steepening at the shelf break associated with oscillating winds (for the plume extent see, e.g., *Piola et al*. [2000, 2008], *Guerrero et al*. [2014], and *Matano et al*. [2014]). Hydrographic stations for transects across the SBF off Patagonia were sampled in the years 1988–1994, 1996, 1997, 2005, and 2006 during different seasons.

Conductivity-temperature-density (CTD) vertical profiles were available for all stations included in our analyses. Absolute salinity, conservative temperature, and derived density from these quantities were computed using the international thermodynamic equation of seawater (TEOS-10) and the MATLAB Gibbs Seawater (GSW) Oceanographic Toolbox from *McDougall and Barker* [2011].

3.2.2. GEF Cruises

In 2005 and 2006, hydrographic stations for transects across the SBF off Patagonia were sampled during Global Environmental Facility (GEF) Patagonia cruises on board R/V ARA Puerto Deseado. Cross-shelf transects were carried out in October 2005 (GEF-1), March 2006, and September 2006 (GEF-3) with a horizontal resolution of ~25 km. CTD profiles for all GEF cruises are available at the National Oceanographic Data Center, and details of the data processing are reported by *Charo and Piola* [2014]. In this work, we present

results from two hydrographic transects acquired during GEF-1 and GEF-3 that were sampled with opposing meridional wind conditions, at ~41°S (off Rincón) and at ~44°S (off Valdés Peninsula).

During GEF-1 and GEF-3 the CTD was equipped with a SeaPoint Chl-a fluorescence sensor. In addition, 5 L water samples were collected with a 12 bottle rosette sampler for analysis of dissolved oxygen and Chl-a concentration among other biological parameters [*Lutz et al*., 2010; *Gómez et al*., 2011; *Segura et al*., 2013; *Perez-Cenci et al*., 2014; *Carreto et al*., 2016]. Water samples were collected at the surface and at 2–3 selected depths (i.e., within and below fluorescence maxima), and Chl-a extraction was performed using a fluorometric method as well as High Performance Liquid Chromatography (HPLC) [*Lutz et al*., 2010; *Carreto et al*., 2016]. Both methodologies showed a significant correlation between Chl-a fluorescence measured by the fluorometer and Chl-a concentration from water samples for all GEF-1 stations. However, *Lutz et al*. [2010] also report that the ratio of Chl-a concentration to fluorescence showed large variability in the vertical and that some stations showed near-surface photo-inhibition.

For the two hydrographic transects presented in this study, some stations were sampled at noon when Chl-a fluorescence can be affected by nonphotochemical quenching, resulting in reduced Chl-a fluorescence at the surface. A linear adjustment of Chl-a fluorescence with Chl-a concentrations extracted from water samples was performed to account for nonphotochemical quenching at the surface. Because not all stations had water samples at depth, we used a linear regression based on all available water samples for each cruise. First, voltage counts measured by the fluorometer were converted to Chl-a fluorescence using scale factors provided by SeaPoint Inc. and offset values determined by measuring the sensor output in the dark. The squared correlation coefficient between Chl-a fluorescence and Chl-a concentration from water samples is $r^2 = 0.69$ for all GEF-1 samples ($N = 163$), and $r^2 = 0.61$ for GEF-3 ($N = 113$). For both cruises, no consistent overestimation or underestimation by the fluorometer was observed. Chl-a fluorescence was recalibrated by multiplying by the slope of a Type I linear regression, forced to intercept zero, between Chl-a concentration from water samples (y axis) and Chl-a fluorescence (x axis). The correction factor was 1.13 for GEF-1, and 0.9 for GEF-3. A Type II regression, which minimizes the distance perpendicular to the regression line, assuming both variables are subject to measurement errors [see, e.g., *Ricker*, 1973], yields qualitatively similar patterns regardless of the method used. Although the magnitude of adjusted Chl-a fluorescence is sensitive to the correction factor, the patterns of Chl-a fluorescence for the three vertical sections analyzed in this study were qualitatively similar. We report adjusted Chl-a fluorescence; however, Chl-a absolute values might not be accurate throughout the water column and should be interpreted with caution.

Because of the coarse horizontal resolution between stations, vertical sections of Chl-a fluorescence were objectively mapped based on the method of *Le Traon* [1990], assuming anisotropic, Gaussian statistics for the eddy field. We used a cross-front length scale of 75 km, based on cross-front autocorrelation of austral spring (September-October-November, SON) satellite Chl-a, and a vertical length scale of 50 m, inferred from the available vertical profiles of adjusted Chl-a fluorescence from GEF-1 and GEF-3 cruises. The data are assumed to have a priori uncorrelated noise, with a noise to signal ratio of 0.25, and interpolated data with error greater than 0.1 were masked.

Shipboard wind observations were recorded during GEF-1 and GEF-3 cruises. For GEF-1, hourly winds recorded at the bridge are available ($N = 19$ for Rincón and $N = 18$ for Valdés transects). During GEF-3, an integrated sampling system made continuous measurements of wind direction and speed. Original data were averaged every 10 min and converted to 10 m winds ($N = 231$ for Rincón transect). These observations, recorded at higher temporal resolution than that of satellite winds, are useful to show directional wind variability during the time periods when the hydrographic transects were sampled. Wind roses for each of these transects were constructed to show the distribution of relative frequencies of wind direction and intensities.

3.2.3. GEF Mooring Site

During the October 2005 cruise, a mooring was deployed at the edge of the continental shelf close to the 200 m isobath. The mooring, located at 43.82°S and 59.67°W, measured meteorological and oceanographic data for 51 days, from 16 October to 5 December 2005.

The mooring acquired high-resolution measurements of meteorological parameters as well as water column temperature and currents throughout the water column. A surface buoy equipped with meteorological

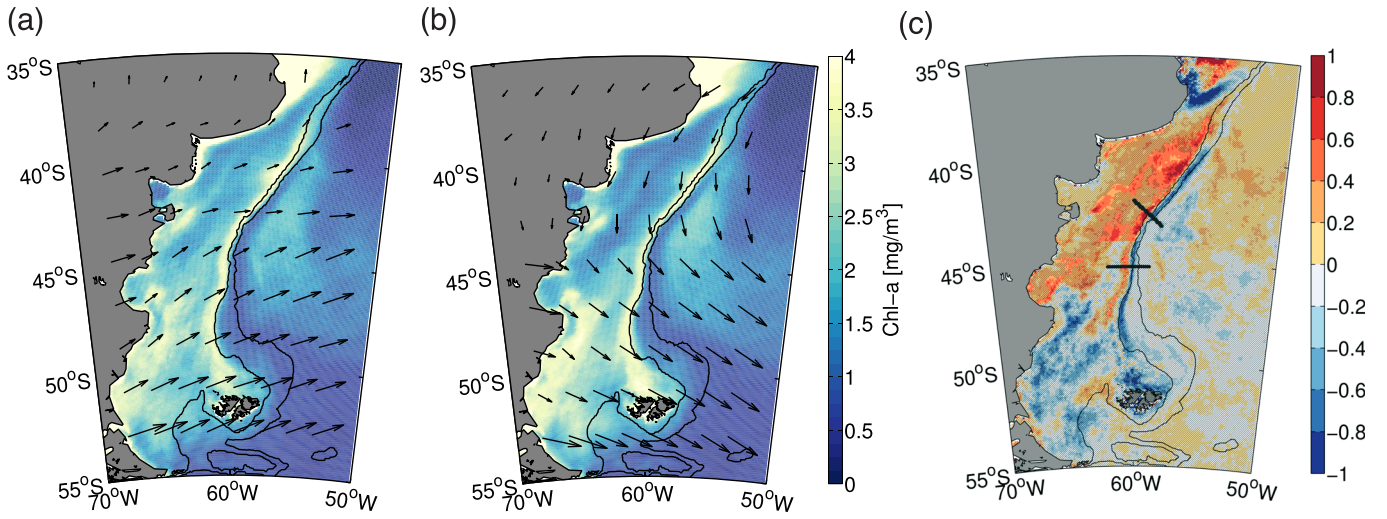

Figure 3. Composites of summer Chl-a for (a) southerly winds and (b) northerly winds, based on 4 day averages of CCMP winds for the period 2000–2011. (c) Difference between Figures 3a and 3b: red implies Chl-a is enhanced for southerly winds relative to northerly winds, and blue indicates enhanced Chl-a with northerly winds. Winds were rotated 35° clockwise north of 44°S to account for the change in the orientation of the sloping bathymetry. Shaded gray areas in Figure 3c indicate that the difference is not statistically significant (i.e., less than the sum of standard errors for maps (a) and (b)).

sensors measured wind speed, direction and gustiness, air humidity, temperature, and pressure. Wind measurements were sampled every second for 10 min intervals centered at the hour. Hourly data were recorded internally and 3 hourly data were transmitted to shore via satellite telemetry in near real-time. Our analyses are based on hourly data. Subsurface temperature and conductivity MicroCAT sensors provided hourly measurements at six depth levels: 1, 10, 30, 50, 75, and 100 m depths. Further details on the buoy specifications and these observations are reported by *Valla and Piola* [2015].

We assess the relationship between meridional winds and in situ temperature at the six depth levels by compositing vertical profiles segregated by along-front wind events as well as by means of a cross-correlation analyses. Cross correlations between meridional winds and temperature are computed from detrended temperature time series (i.e., removing a linear trend from temperature at 1, 10, and 30 m only, as during the analysis period there was no significant linear trend below 30 m) that were band-pass filtered to remove variability on temporal scales shorter than 1 day observed in autocorrelations (i.e., diurnal at 1 m and semidiurnal at 75 and 100 m associated with tides), and longer timescales (i.e., $>$10 days) for which few realizations are present in the record (i.e., 51 days). Detrended temperature time series were band-pass filtered using running means, i.e., a (24 $\times$ 5)-h running mean was subtracted from the low-pass temperature data that retained variability on scales longer than 1 day (i.e., by applying a 12 h running mean). Prefiltering the data is expected to improve statistical reliability when correctly accounting for the effective number of degrees of freedom [*Davis*, 1977; *Pyper and Peterman*, 1998]. The significant correlation at 95% confidence was computed adjusting the number of degrees of freedom considering the autocorrelation of meridional winds and temperature data following *Bretherton et al.* [1999], which results in a critical correlation coefficient equivalent to subsampling the filtered time series every 48 h.

4. Results and Discussion

4.1. Composites of Satellite Chl-a by Wind Direction

To investigate the impact of along-front winds on Chl-a variability at the SBF, we first looked at composites of satellite Chl-a, segregating the data by wind direction (Figure 3). We use summer data here, because in the summer phytoplankton growth is presumed to be nutrient limited, and previous correlation analyses showed wind speed and satellite Chl-a to be correlated in summer in this region [*Carranza and Gille*, 2015], while correlations are weak and nonsignificant in other seasons. Each satellite Chl-a grid cell was screened for positive (i.e., southerly) or negative (i.e., northerly) along-front winds. Because north of $\sim$44°S the shelf break does not have a north-south orientation (see Figure 1), we rotated winds 35° clockwise north of 44°S

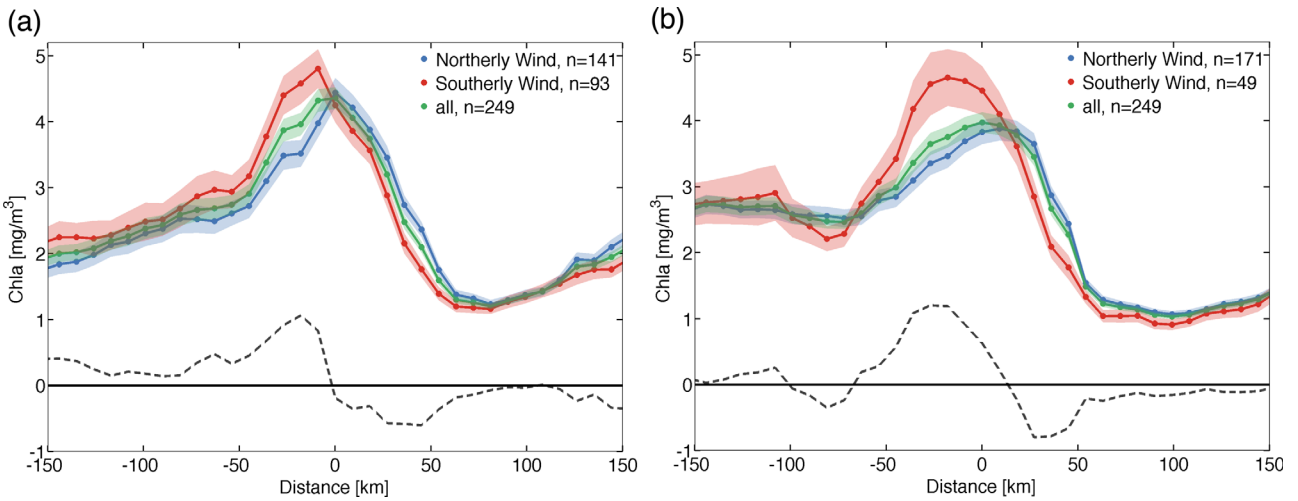

Figure 4. Mean summer satellite Chl-a for southerly winds (red), northerly winds (blue), and all summer cases (green) for the two transects across the shelf-break front shown in Figure 3c, in the (a) northern sector and (b) southern sector. The dashed gray line shows the difference between red and blue lines. The *x* axis is the distance from the shelf-break front, defined as the pixel where mean summer Chl-a peaks (maximum in the green line).

and used meridional winds south of that latitude. Mean satellite Chl-a maps for along-front southerly winds, northerly winds, and the difference between the two are shown in Figure 3.

Over the shelf break, onshore of the 200 m isobath, southerly winds are associated with enhanced satellite Chl-a (red in Figure 3c). Further offshore northerly winds are associated with high Chl-a (blue band offshore of the 200 m isobath in Figure 3c). The red band of high Chl-a for southerly winds at the SBF is statistically significant (i.e., the difference is larger than the sum of standard errors for mean Chl-a maps). Offshore of the mean position of the SBF, Chl-a is enhanced with northerly winds, and, although the difference shown in Figure 3c is not statistically significant, because Chl-a is generally low, the spatial pattern is consistent along the length of the shelf break suggesting this is a real pattern rather than noise. This large-scale pattern emerges when we consider along-front winds, and there is no pattern associated with cross-front winds, implying no clear response of Chl-a to the relaxation of along-front winds. Differences are more pronounced if we consider only along-front winds that are larger in magnitude than the cross-front wind component. However, because fewer cases meet these criteria, the statistically significant red band shows less spatial consistency (not shown). The same pattern also arises in correlation maps between anomalies of along-front winds and Chl-a at zero lag (not shown), but we present the composites to ease the interpretation.

The pattern of consistently high Chl-a or low Chl-a to either side of the SBF is more remarkable in summer than during the other seasons. To better illustrate the cross-front shift in satellite Chl-a with changing along-front wind direction, in Figure 4, we compare mean Chl-a for all summer cases (in green) against mean Chl-a for southerly winds (red) and northerly winds (blue) for two cross sections at the SBF, indicated by black lines in Figure 3c. Cases of southerly wind are less frequent than cases of northerly wind, because north of 50°S mean summer winds present a northerly component (see Figure 1b), but in both of these transects, the Chl-a peak is shifted onshore of the SBF (i.e., defined here as the peak in the green curve) with southerly winds, and the difference between Chl-a concentrations for southerly winds and northerly winds is significant compared with the overall summer mean. This wind-related cross-front shift in the location of the Chl-a peak suggests the influence of cross-front Ekman transport interacting with the sloping isopycnals at the front. In addition, the Chl-a difference between southerly and northerly wind composites is largest near the SBF and diminishes further away from the SBF (dashed gray curve in Figure 4).

Increased Chl-a at the SBF with southerly winds is consistent with the concept that enhanced upwelling at the shelf break occurs when Ekman transport is expected to move near-surface waters onshore (i.e., with southerly winds in the SH) and steepen isopycnals, as proposed by *Siedlecki et al*. [2011]. On the other hand, northerly winds associated with high Chl-a offshore of the 200 m isobath may indicate upwelling of nutrients from the BBL, through isopycnal tilting, enhancing phytoplankton growth further offshore.

However, satellite observations do not allow us to determine whether the surface signal results from surface advection of high Chl-a from shelf waters by Ekman transport or from isopycnal upwelling that would supply nutrients and enhance growth and/or upwell Chl-a from a subsurface maximum further offshore.

4.2. Isopycnal Tilting, Changes in Stratification, and In Situ Chl-a: Synoptic Evidence

Ship-based hydrographic surveys provide a means to evaluate snapshots of the vertical structure across the shelf break. Several in situ hydrographic transects across the SBF were occupied during predominantly along-front wind events. We contrast the southerly and northerly wind cases. In all cases density sections show isopycnal tilting in agreement with induced Ekman transport at the surface, but because many were sampled in different years and/or in different seasons they are not easily compared. In this section we present two synoptic hydrographic transects across the SBF, off Rincón (at ∼41°S) and Valdés (at ∼44°S), selected because they were occupied during the same cruise, but with opposing wind directions. This allows us to look at isopycnal tilting due to oscillating along-front winds. On 10 October 2005, Rincón was sampled during a northerly wind event (Figures 5a and 5b), then winds reversed direction and became from the south when Valdés was sampled on 15 October (Figures 5c and 5d). Because they were sampled 4–5 days apart in October 2005, and they are only 300 km apart, mean background hydrographic conditions were likely similar. A year later, in 23–25 September 2006, Rincón was reoccupied when winds had reversed relative to October 2005, and it was sampled during a southerly wind event (Figures 5e and 5f). For all three occupations, the CTD carried a fluorometer from which an estimate of Chl-a concentration can be derived (see section 3.2 for details).

Mean satellite winds and Chl-a maps and vertical sections of adjusted Chl-a fluorescence with isopycnals overlaid in white contours for the three occupations are shown in Figure 5. For northerly winds (Figures 5a and 5b), flattened isopycnals are consistent with surface waters moving offshore in the Ekman layer. For southerly winds (Figures 5c–5f), isopycnals tilt upward, which could result from onshore Ekman transport in the surface layer.

The analysis of water mass properties for stations at the shelf break for these sections supports this hypothesis (Figure 6). There are pronounced differences in the temperature-salinity (TS) structure at the shelf-break stations between sections sampled during northerly wind and southerly wind events. Rincón's station at the SBF occupied during northerly winds shows a much warmer, fresher upper layer and a slightly colder, saltier bottom layer (red), than the station at the SBF occupied during a subsequent southerly wind event (light blue). The change in the vertical thermohaline structure corroborates the offshore flux of warm-fresh shelf water in the upper layer and the compensating onshore flux of cold-salty slope water during the northerly wind event. The reoccupation of Rincón with southerly winds (blue) shows no evidence of shelf waters at the surface and much colder, saltier water at depth. (Although this station was deeper, we only show the upper 150 m to facilitate visual comparison.)

Offshore Ekman transport in the surface layer (i.e., northerly wind case), flattens the isopycnals, and may imply an onshore flux of nutrient-rich waters from the Malvinas Current at depth (or onwelling). Conversely, onshore Ekman transport (i.e., southerly wind case), steepening the isopycnal slopes, can potentially pump nutrients from the bottom-boundary layer to the surface enhancing phytoplankton growth and accumulation at the SBF, as suggested by *Siedlecki et al*. [2011]. The Chl-a fluorescence signal is consistent with surface Chl-a enhancement further offshore for the case of northerly winds (Figure 5b), suggesting upwelling along the sloping density layers from the bottom to the surface. With southerly winds (Figures 5d and 5e), Chl-a is enhanced at the SBF, consistent with onshore Ekman transport and vertical isopycnals that would enhance upwelling, delivering nutrients to the surface.

To illustrate the spatial extent of the Chl-a signal at the surface, the left panels of Figure 5 show satellite Chl-a at the time when the transects were sampled. On 10 October 2005, the northern sector of the SBF was cloudy, and satellite Chl-a could not be retrieved; instead we show 3 day averaged satellite Chl-a. In the northern sector of the shelf break and during the predominantly northerly wind event, the band of high Chl-a extends offshore of the 200 m isobath (Figure 5a). The enhanced vertical stratification associated with offshore flow of less dense shelf waters and onshore flow of denser slope waters below the Ekman layer may prevent the upwelled water from reaching the surface at the shelf break. Thus, the highest Chl-a fluorescence is observed below the surface mixed layer (∼22 m). After winds reversed direction, the high band of Chl-a shifts onshore (Figure 5c). This band of high satellite Chl-a is also apparent in the Chl-a anomaly

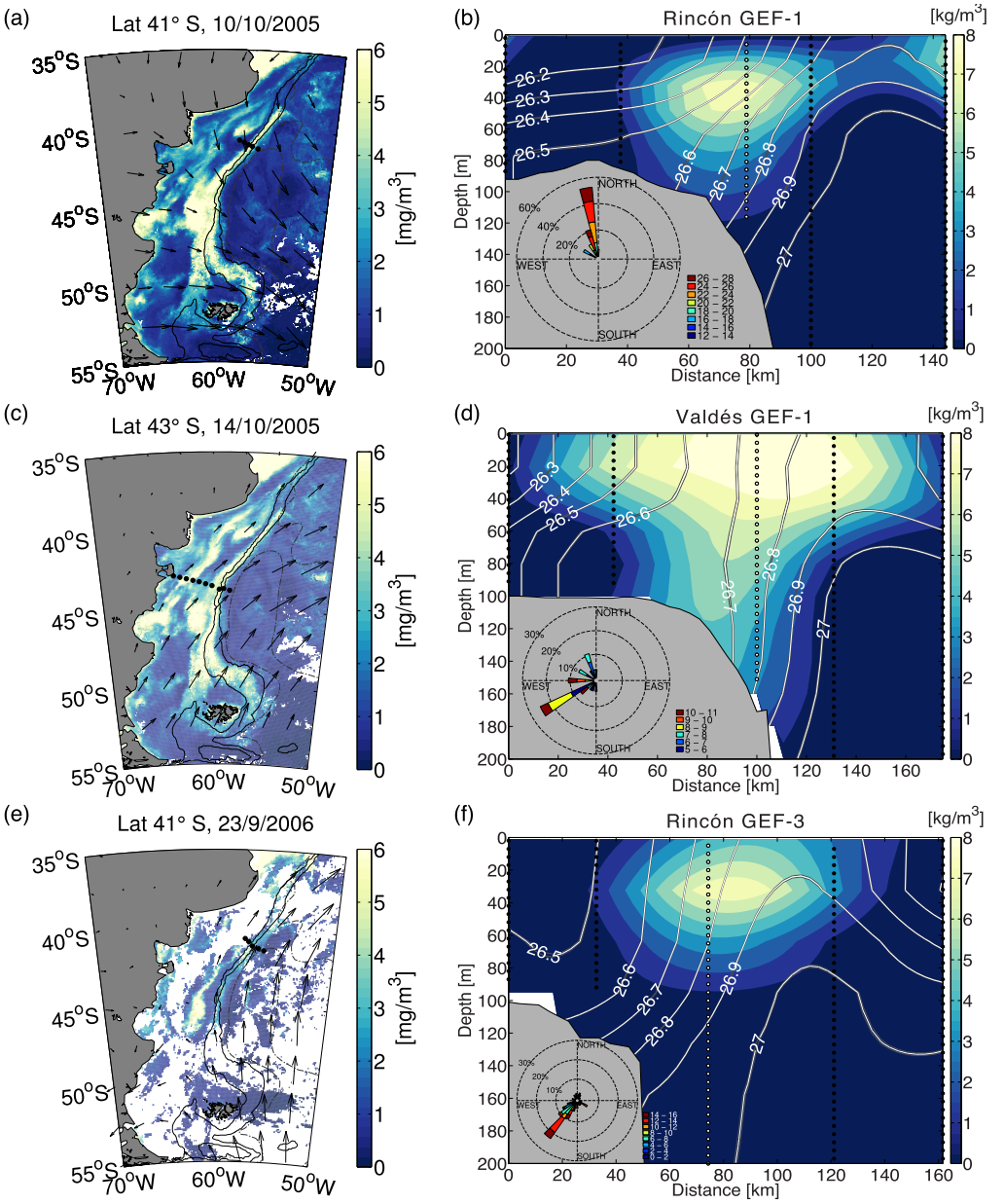

Figure 5. Satellite Chl-a and surface winds (left), vertical structure of adjusted Chl-a fluorescence (right, color bar) with density contours overlaid in white, for two transects across the shelf break. (a, b) The northern transect (Rincón) was sampled on 10 October 2005, when winds were predominantly from the north. (c, d) After 4 days, winds reversed direction and the southern transect (Valdés) was sampled on 15 October 2005 over the shelf-break. (e, f) Rincón was revisited on 23–25 September 2006 when winds were from the south. Vertical sections were objectively mapped (see section 3.2.2) and values with uncertainty higher than 0.1 are masked. Black dots in the map and vertical sections indicate the location of hydrographic stations. White dots identify stations in the TS diagram of Figure 6. Wind roses in Figures 5b, 5d, and 5f show the relative frequency of wind directions by wind speed ranges (in m s^{-1}) during each transect sampling period, based on hourly (GEF-1) and 10 min (GEF-3) shipboard wind observations.

maps relative to the climatological monthly mean for October (not shown). Cloud cover precludes a regional analysis of the surface Chl-a signal in September 2006.

4.3. Isopycnal Tilting and Changes in Stratification: Statistical Significance

Hydrographic transects in Figure 5 provide evidence of isopycnal tilting with along-front wind reversals, but they only represent snapshots of water column structure for selected cruises. In this section we present composite hydrographic sections for southerly and northerly winds to assess the statistical significance of

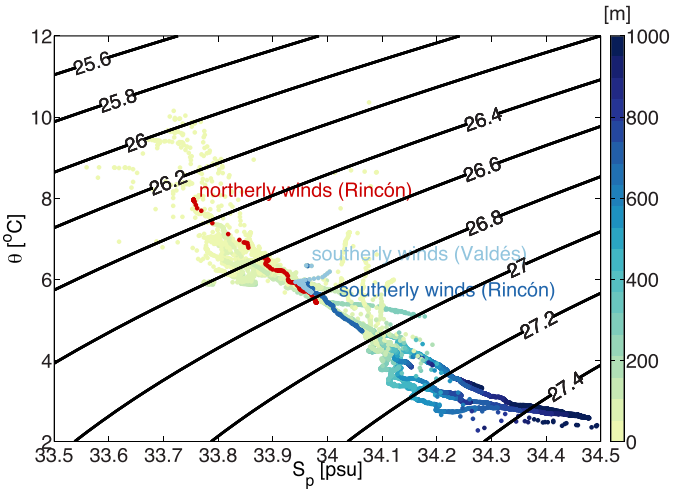

Figure 6. Temperature-salinity (TS) diagram for stations at the shelf break indicated with white dots in vertical sections of Figure 5. In red: Rincón station at the SBF sampled with northerly winds on 10 October 2005 (for reference, station 11 from GEF-1), in light blue: Valdés station at the SBF sampled with southerly winds on 14 October 2005 (station 35 from GEF-1), and in blue: Rincón station at the SBF sampled during a southerly wind event on 23–25 September 2006 (station 53 from GEF-3). All stations at the SBF between 39°S and 44°S, deeper than 100 m and shallower than 1500 m, are shown as reference, with the color bar indicating depth.

isopycnal tilting due to along-front changes in the wind. In Figure 7, we show mean austral winter and spring (June–November, JJASON) density sections across the SBF, with stations segregated by wind direction. In summer (DJF), strong stratification develops, the SBF is density-compensated and, therefore, the dynamical response of the front to along-front winds is less remarkable (not shown). Also, winds in the summer tend to be from the north and there are few cases of profiles sampled with southerly winds to evaluate the response of the SBF to changes in along-front winds.

To construct mean hydrographic transects (Figure 7), for each hydrographic station we assigned a wind vector by collocating vertical profiles with satellite rotated winds in space (within 25 km of the satellite grid) and time (within 6 h of the satellite wind estimate). Stations were then segregated by either positive or negative along-front wind component. For comparison with no-wind conditions, for these transects, only cases when the along-front wind component was greater than 2 m s^{-1} were considered for either northerly ($N = 73$ profiles) or southerly winds ($N = 94$). Cases when along-front winds were less than 2 m s^{-1} were flagged as "calm" (i.e., relatively weak along-front winds), and mean density contours for calm conditions

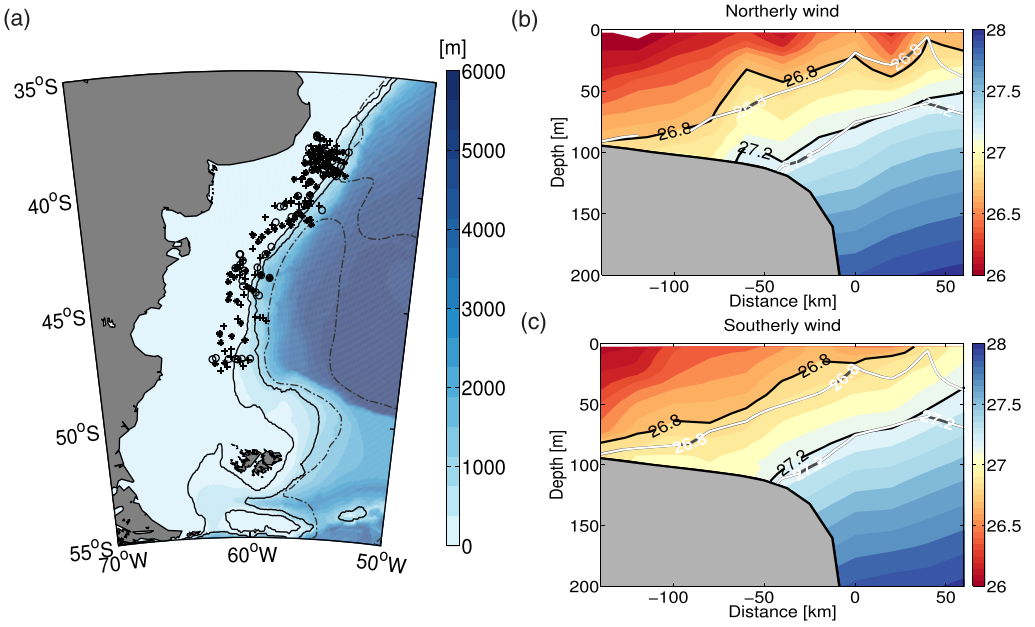

Figure 7. (a) Location of historical hydrographic stations between 38°S and 50°S sampled with northerly (⋆), southerly (+), and no-wind conditions (°), used in mean hydrographic density sections for (b) northerly winds ($N = 78$) and (c) southerly winds ($N = 94$) in winter and spring (JJASON). To segregate profiles, here, we used a threshold of 2 m s^{-1} for the intensity of along-front winds. Cases when the along-front wind component was less than 2 m s^{-1} were considered "calm," although stronger cross-front winds could occur in these cases. Mean density contours for calm conditions ($N = 67$) are overlaid in white.

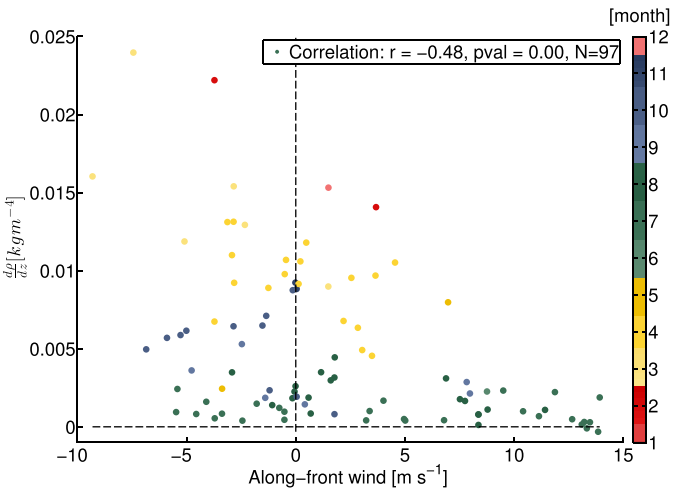

Figure 8. Scatterplot for the density gradient between 100 m and the surface versus the along-front wind component, for stations between 38°S and 44°S. The correlation for the 97 stations at the SBF with CCMP wind data is −0.48, significant at the 99% level. The color bar shows the month of the year.

($N = 67$) are overlaid in white for reference in Figure 7b and 7c. Mean density transects across the SBF were computed using *Linder et al.* [2004]'s algorithm, which bins profiles according to cross-shelf distance from a given isobath to compute mean cross-shelf sections of hydrographic properties in regions of sloping bathymetry. We modified the algorithm to use a version of the General Bathymetric Chart of the Oceans (GEBCO) bathymetry field that has been corrected based on soundings from cruises, gridded at 3 min resolution (0.05° latitude and longitude). As a reference bathymetry line, for averaging profiles we use the 200 m isobath, which corresponds to the mean position of the SBF off Patagonia.

The mean density section for stations sampled with southerly winds (Figure 7c) shows surfacing isopycnals tilted upward relative to the mean density section for stations sampled with northerly winds (Figure 7b). The surfacing of isopycnals for northerly winds occurs further offshore than for southerly winds (Figure 7), although the foot of the front, defined here as the grounding of the isopycnals between 26.8 and 27.2 kg m^{-3}, does not show substantial displacement. For example, the outcrop of isopycnal 26.8 that occurs near the 200 m isobath with southerly winds occurs ∼50 km offshore with northerly winds. The migration of the foot of the front is difficult to assess because of inhomogeneities of the bathymetry along the 200 m isobath and the averaging procedure. In addition, the foot of the front is expected to lag changes in the winds by a few days [*Siedlecki et al.*, 2011]. Nonetheless, the surface expression of the sloping isopycnals with changing along-front winds is a robust feature that shows in mean density sections for winter and spring.

Ekman transport can displace waters to either side of the front, modifying the stratification of the surface layer either by destratifying (i.e., with southerly winds) or restratifying (i.e., with northerly winds). As a measure of stratification, we computed the vertical density gradient between 100 m and the surface for stations within 50 km of the 200 m isobath. The vertical density gradient versus along-front wind component is shown in Figure 8, for stations in the latitude range between 38°S and 44°S. We find a negative correlation between stratification and the along-front component of the wind in agreement with theory: northerly winds (i.e., $V < 0$) typically result in more stratified waters in the upper 100 m, whereas southerly winds (i.e., $V > 0$) are associated with lower stratification. Although the correlation is low ($r = -0.48$, based on $N = 97$), it is statistically significant at the 99% level. Selecting a smaller latitudinal range yields higher significant correlations (with $N > 50$), and r varies between −0.3 and −0.7 with lower correlations south of 45°S, where bathymetric contours spread out and stratification is generally low due to large tidal amplitudes [*Combes and Matano*, 2014].

4.4. Water-Column Response to Along-Front Winds

The mooring deployed at the shelf break in the location indicated in Figure 9a allows us to assess the water-column response to oscillating meridional winds, providing high-resolution information in the temporal domain. The time series of meridional winds and surface water temperature anomalies (i.e., subtracting a linear trend) are shown in Figure 9. Decorrelation scales of meridional winds and temperature for this record are similar (∼48 h); however, measurements from a different period (presented in *Valla and Piola* [2015], for which subsurface temperature measurements at depth were not available) show that meridional winds typically decorrelate faster (∼24 h). The wind record in Figure 9 shows several periods of oscillating meridional winds: wind reversals at 4–5 day intervals seem to dominate during part of the record, 25 October to 15 November 2005, but before and after this time period the wind appears to reverse at shorter timescales.

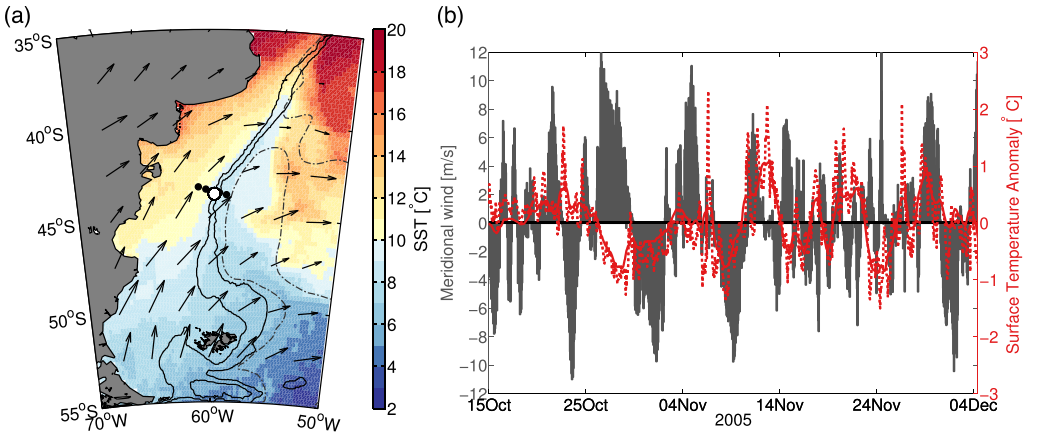

Figure 9. (a) Mean sea surface temperature (color bar) with wind vectors overlaid for the period 16 October to 5 December 2005, when the mooring site at ~ 44°S indicated by the white dot acquired hourly winds and water column temperature at six depth levels from the surface to 100 m (bottom depth at 185 m). (b) Time series of meridional winds (gray) and detrended sea surface temperature anomalies (red) at the mooring site indicated by the white dot in Figure 9a. Positive meridional winds indicate southerly winds, and negative meridional winds indicate northerly winds. For correlation statistics between along-front winds and temperature see Figure 10.

The oscillating meridional winds are correlated with water temperature in the upper 100 m (where temperature measurements are available). Following a period of southerly winds (i.e., positive meridional winds), temperature decreases. Lagged cross correlations between meridional winds and water column temperature anomalies show a coherent signal at the six depth levels (Figure 10). Positive lags imply that wind leads changes in temperature, and the negative correlation for the first significant peak is consistent with southerly winds associated with cold temperatures at the front, which is consistent with local upwelling. Cross correlations show that temperature responds to changes in the winds with a lag of ~2–4 days, in agreement with response timescales of the density field due to along-front winds from numerical simulations [*Siedlecki et al.*, 2011; *Moffat and Lentz*, 2012; *Zhang et al.*, 2014]. Mixed-layer depth estimates from the mooring record give a mean value of 33 m, using temperature and density threshold criteria from *de Boyer Montégut et al.* [2004], with a standard deviation of 9 m. Lagged cross correlations between meridional winds and temperature show a consistent pattern beyond the surface mixed layer, indicating water-column structure changes due to advective isopycnal tilting.

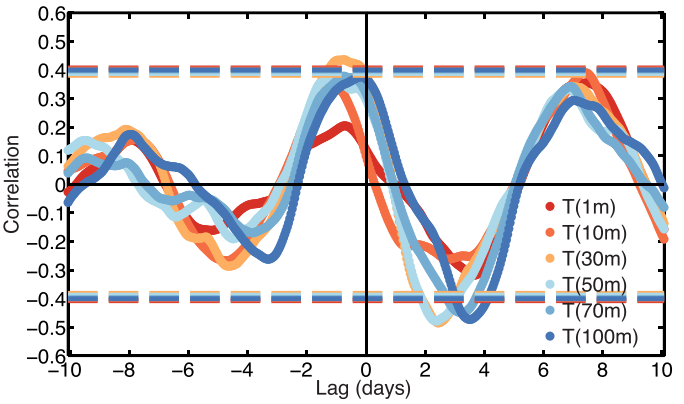

Figure 10. Lagged cross correlations between meridional winds and detrended (i.e., removing the linear trend) and band-pass filtered (i.e., retaining variability in the 1–10 day band) temperature at the six depth levels measured (see legend). Positive lags indicate wind is leading with respect to changes in water temperature. A negative correlation for the first significant peak implies southerly winds are associated with cold temperatures. The 95% confidence interval for significant correlations (indicated by the dashed lines) was computed adjusting the degrees of freedom based on autocorrelations of meridional winds and temperature anomalies, following *Bretherton et al.* [1999].

The water-column temperature, salinity, and density structure also show a much more homogeneous water column after southerly winds (blue in Figure 11), in contrast to a more stratified water column after a period of northerly winds (red in Figure 11). To illustrate this, in Figure 11 we show mean profiles estimated during 24 h periods following persistent wind events that lasted more than 1.5 days. This criterion results in two southerly wind events and five northerly wind events for the 51 day record. Selecting wind events with a minimum duration of 1 day, results in a larger number of events (four southerly wind events and eight northerly wind events) and shows a qualitatively similar structure (not shown), but differences are more

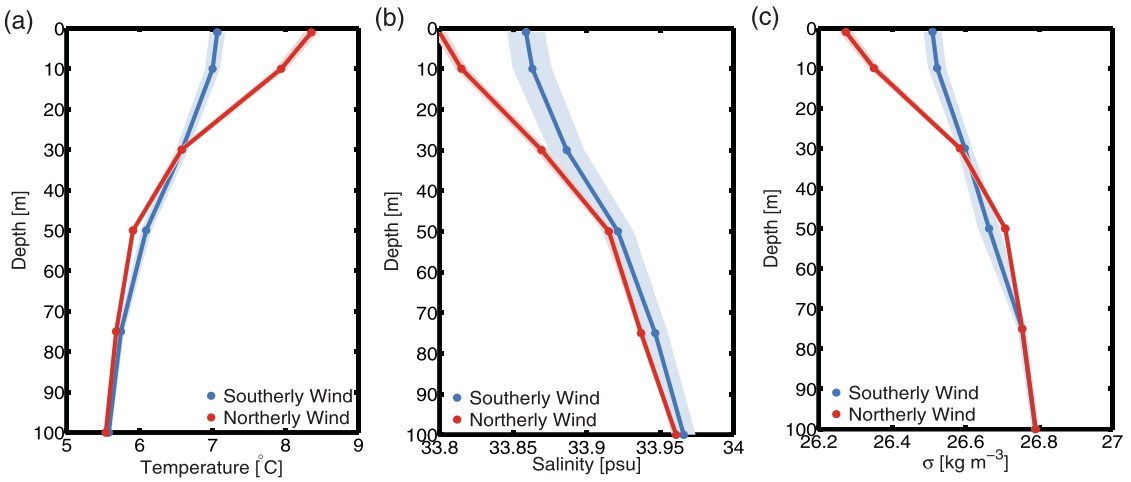

Figure 11. Mean (a) temperature, (b) salinity, and (c) density profiles at the mooring location (bottom depth at 185 m), averaged over a 24 h period at the end of southerly wind events (in blue), and northerly wind events (in red). The colored shading indicates the standard error. A southerly wind event was identified when positive winds persisted for more than 1.5 days, and a northerly wind event when negative winds persisted. This resulted in two southerly wind events ($N = 48$) and five northerly wind events ($N = 120$).

pronounced when considering wind events that lasted more than 1.5 days. The longest southerly wind event in the record lasted more than 3 days (73 h), in late October 2005. Mean temperature, salinity, and density profiles for the last day of that event (i.e., on 29–30 October 2005) show no traces of shelf waters at the surface (e.g., $S_p > 33.8$ psu over the entire water column), and a thoroughly mixed water column in the top 100 m (not shown). Differences in surface density between northerly and southerly wind events are on average 0.25 kg m^{-3} and exceed 0.4 kg m^{-3} for the events of longest duration (i.e., the above mentioned southerly wind event, and a northerly wind event that ended on 11 November 2005 and lasted 3.6 days).

5. Further Discussion

We have shown evidence for wind modulation of upwelling and Chl-a concentrations at the SBF off Patagonia from a diverse set of observations that include satellite observations and in situ measurements. The wind modulation at the SBF is associated with the along-front component of the winds, and it is consistent with the theory of enhanced shelf-break upwelling and the nutrient pumping mechanism postulated by *Siedlecki et al*. [2011]. We find that southerly winds (i.e., downfront) enhance satellite Chl-a at the SBF off Patagonia, destratify the water column and tilt isopycnals upward, possibly allowing for enhanced nutrient supply to the euphotic zone. Conversely, northerly winds are associated with enhanced stratification and flatter isopycnals, preventing nutrients and/or a subsurface Chl-a maxima from reaching the surface at the SBF but enhancing surface Chl-a further offshore. Some results pointing in this direction deserve further discussion.

The amplitude modulation of the satellite Chl-a signal by along-front winds is $<\pm 1$ mg m^{-3} (Figure 3c), but the magnitude is likely underestimated for several reasons. (1) Our satellite-based results pertain to summer, when strong stratification may prevent the movement of the foot of the front and inhibit the nutrient pumping effect [*Siedlecki et al*., 2011]. The amplitude modulation of satellite Chl-a by along-front winds is incipient in the spring (not shown), though factors other than nutrient limitation (e.g., light limitation and zooplankton grazing) can influence phytoplankton growth and/or accumulation at the surface and may explain the seasonal differences in the Chl-a response. (2) In either season, an oscillation in along-front winds is required to pump water effectively from the near-bottom layer and the ocean interior to the ocean surface, and our satellite results based on Chl-a composites, can include northerly and southerly wind events that were not necessarily followed by a subsequent wind reversal persistent enough to allow time for the pumping mechanism to take place or its effects to reach the sea surface. (3) Although modeling studies have shown surface phytoplankton biomass at fronts is largely controlled by enhanced nutrient supply during wind events, the strongest phytoplankton response to wind-driven frontal dynamics is expected to occur at the subsurface [*Franks and Walstad*, 1997; *Nagai et al*., 2008; *Whitt et al*., 2017]. Subsurface phytoplankton blooms deeper than one optical depth, which are a common feature of fronts (see, e.g., subsurface

blooms in Figures 5b and 5f) and can occur particularly in summer [e.g., *Franks and Walstad*, 1997; *Hales et al*., 2009], will be missed by satellite radiometers [e.g., *Morel and Berthon*, 1989] and upwelling along the front could still be happening. Thus, the phytoplankton response to wind-front dynamics from satellite Chl-a is likely underestimated [*Franks and Walstad*, 1997].

Nonetheless, a clear signal emerges from composites of satellite Chl-a from all cases of northerly versus southerly winds. The effect of subsequent along-front wind reversals in the water-column vertical structure, cross-front density structure, and Chl-a fluorescence signal is depicted by the two synoptic transects sampled during the GEF-1 cruise (Figure 5) as well as by the observations at the mooring site (Figures 10 and 11). For persistent wind events followed by persistent wind reversals, the amplitude modulation of the Chl-a signal is expected to be larger, e.g., differences in surface Chl-a fluorescence can be greater than 5 mg m^{-3} (Figures 5b and 5d). The Chl-a amplitude modulation due to along-front oscillating winds is significant compared to the ~4 mg m^{-3} for the annual amplitude (Figure 1b).

The cross-front displacement of the satellite Chl-a peak due to changing wind conditions is relatively small (i.e., ~25–50 km), but large enough to be detectable from satellite observations and coarse resolution hydrographic transects. An offshore displacement of the high satellite Chl-a band at the SBF, relative to the 200 m isobath, from early spring to late summer, was reported by *Romero et al*. [2006], which could be related to the increased frequency of northerly wind events (and associated offshore Ekman transport) during the summer season.

The Chl-a response to alongshore winds might appear to conflict with results reported by *Saraceno et al*. [2005], who found that strong northerly winds lead to higher Chl-a in the northern part of the shelf and SBF, where our Figure 3c shows red, implying higher Chl-a with southerly winds. However, their analysis focused on seasonal to interannual timescales, and by low-pass filtering, they suppressed the high-frequency wind variability that is the focus of this study. The differing correlation patterns suggest that different mechanisms operate on synoptic versus longer timescales.

Valla and Piola [2015] also carried out an independent assessment based on surface currents and temperature observations from another mooring at the SBF off Patagonia. Their results agree with ours in showing that high-frequency variability (i.e., subseasonal) surface cooling events, linked to intense upwelling, lead to a significant increase in surface Chl-a at the SBF. Although their analysis does not include the effect of directional wind forcing, the intense cooling event they reported in January 2007 was coincident with southerly synoptic winds over the shelf break (their Figure 13). They also reported onshore surface velocities prior to the cooling period and offshore velocities near its termination (~13–15 cm s^{-1}). Although the magnitude of the upwelling inferred from that event is in agreement with predictions from numerical experiments with realistic boundary conditions and forcing [*Combes and Matano*, 2014], as *Valla and Piola* [2015] pointed out, the timescales over which the cooling events occur in the model and observations do not agree (i.e., ~180 versus ~5 days, respectively). Numerical simulations from *Combes and Matano* [2014] also suggested that the upwelling at the SBF off Patagonia is not sensitive to changes in local wind forcing, but these experiments were forced with monthly climatological mean winds that did not resolve the atmospheric synoptic activity. The timescales and duration of the cooling events reported by *Valla and Piola* [2015] (i.e., 3–18 days) are in closer agreement with wind-driven upwelling by along-front wind synoptic variability.

While changes in wind speed can lead to changes in vertical mixing, regardless of the direction of the wind, and thus can have an impact on Chl-a accumulation [e.g., *Carranza and Gille*, 2015], in this region, correlations between wind speed and Chl-a anomalies show relative minima [see *Carranza and Gille*, 2015, Figure 7a], and the enhancement of Chl-a at the SBF differs depending on wind direction. Thus, wind-speed-induced vertical mixing does not appear to be a dominant mechanism in the Patagonia SBF. The lack of correlation between surface Chl-a and cross-front or zonal winds at the SBF (not shown), further supports *Siedlecki et al*.'s [2011] theory, indicating that atmospheric synoptic storms, which are associated with fluctuations in meridional winds with periods between 2 and 10 days [e.g., *Vera*, 2003], can significantly enhance upwelling at the SBF off Patagonia, and also potentially at other shelf-break fronts of western boundary currents. For example, the modification of the density structure due to along-front wind oscillations in the synoptic band was identified in observations from the New England SBF sector of the MAB [*Aikman et al*., 1988; *Houghton et al*., 1988; *Fratantoni and Pickart*, 2003]. However, despite persistent upwelling revealed from observations in the MAB, there is no persistent Chl-a enhancement at the SBF, possibly due

to zooplankton grazing [*Zhang et al*., 2013]; baroclinic instabilities of the jet cause significant current variability [*Fratantoni and Pickart*, 2003]. The mechanism proposed by *Siedlecki et al*. [2011], who neglected along-shelf pressure gradients, may be applicable in the Patagonian shelf, due to the barotropic nature and stability of the Malvinas Current [*Vivier and Provost*, 1999; *Piola et al*., 2013], the relative low meandering and eddy kinetic energy observed [*Goni et al*., 2011; *Artana et al*., 2016], and the predominantly meridional orientation of the bathymetry.

Wind-induced upwelling in the vicinity of a jet may also be caused by along-front wind stress variations in the cross-front direction [*Lee et al*., 1994; *Zhang et al*., 2011], which can be induced by the surface current itself even under uniform wind forcing. Assuming uniform winds that are stronger in magnitude than the surface current jet, the differential along-front wind stress to either side of the front can produce Ekman transport divergences and upwelling through Ekman pumping. Such a mechanism would lead to upwelling onshore of the SBF, regardless of wind orientation: for southerly winds the effective stress is minimum at the core of the jet leading to smaller Ekman transport onshore relative to either side of the jet, while for northerly winds, a maximum wind stress at the jet core would lead to greater offshore Ekman transport at the jet. In both cases, this results in surface divergence and upwelling onshore of the Malvinas Current jet. However, our results suggest that onshore of the Patagonian SBF, upwelling is enhanced with southerly winds but suppressed with northerly winds. This is likely due to the fact that in this region winds are generally much stronger than surface currents, thus the impact of the surface currents on the effective stress is minimal.

Nutrient distributions for the synoptic transects presented in this study are reported by *Carreto et al*. [2016, Figure 5], who show higher nutrient concentrations at the SBF for the southerly wind case (i.e., Valdés, see Figures 5c and 5d) compared with the northerly wind case (i.e., Rincón, see Figures 5a and 5b), in agreement with the results presented here. Due to the lack of concomitant observations of nutrients, vertical diffusivities and/or vertical velocities, a meaningful assessment of the upwelled nutrient fluxes associated with the along-front wind induced upwelling [e.g., *He et al*., 2011] is not feasible. Although the existing nutrient data combined with the approach of *Valla and Piola* [2015] to estimate vertical velocities from the mooring site may prove useful for an estimate of the upwelled flux of nutrients, quantifying the role of this mechanisms is out of the scope of this study but will be the focus of future work.

6. Conclusions

This work has demonstrated that wind forcing on subseasonal timescales is important for shelf-break exchange and can lead to enhanced upwelling and Chl-a concentrations at shelf-break fronts of western boundary currents. We presented observational evidence that wind modulates the upwelling at the shelf-break front off Patagonia, consistent with a mechanism for nutrient pumping associated with along-front wind oscillations that was proposed by *Siedlecki et al*. [2011] based on a numerical model. Composites of satellite Chl-a segregated by wind direction, hydrographic transects with Chl-a fluorescence across the shelf-break front sampled with opposing wind direction, and a mooring site that collected high-resolution wind and hydrographic data throughout the water column suggest that oscillations in along-front winds can modulate the vertical stratification and the upwelling at the shelf-break front off Patagonia, with biological implications. Atmospheric synoptic scale storms, characterized by fluctuations in meridional winds with periods between 2–10 days, can potentially induce shelf-break upwelling at other shelf-break fronts at the western margins of ocean basins.

For the 1500 km long Patagonian SBF extending roughly meridionally, the theory predicts that southerly winds (downfront), lead to Ekman transport onshore in the surface layer and tilt isopycnals upward, destratifying the water column and allowing upwelling of nutrients from deeper layers. Conversely, northerly winds (upfront) lead to offshore Ekman transport, flatten isopycnals, stratify the water column at the front and prevent nutrients and/or Chl-a from a subsurface maximum from reaching the surface. In agreement with theory, satellite observations show that surface Chl-a is enhanced at the SBF (i.e., onshore of the 200 m isobath) with southerly winds, and suppressed with northerly winds when surface Chl-a is enhanced further offshore (i.e., ∼25–50 km). The Chl-a amplitude modulation by along-front winds inferred from satellite observations (in summer) is ∼25% of the mean annual Chl-a amplitude for the 12 year satellite record. Hydrographic transects from synoptic surveys as well as mean density sections from historical observations segregated by

along-front wind direction, are also consistent with the theory. However, the Chl-a fluorescence difference between subsequent changes in along-front wind direction can be significantly larger in the spring ($\pm$5 mg m^{-3}), compared to the summer estimate from satellite observations. Nutrient distributions for the synoptic transects presented in this study [*Carreto et al*., 2016] are in accord with the theory. High-resolution (i.e., hourly) wind and water column hydrographic time series collected in spring at the mooring site provide further evidence and show that southerly winds destratify the water column leading to cooling events, whereas northerly winds restratify the upper ocean and lead to warming events. Most importantly, the timescale for the water column response to changes in along-front winds inferred from the mooring site (i.e., 2–4 days) is consistent with the timescale response predicted from numerical experiments [*Siedlecki et al*., 2011; *Moffat and Lentz*, 2012; *Zhang et al*., 2014].

Recognizing the limitations of the existing observations at the SBF of Patagonia, we have focused on presenting robust patterns of variability that indicate along-front wind-induced upwelling through the Chl-a response in a qualitative sense. A meaningful quantification of the upwelled nutrient fluxes, associated with the upwelling induced by along-front wind oscillations, requires water-column concomitant observations of nutrient concentrations, vertical diffusivities and velocities for the three wind scenarios (i.e., northerly, southerly and calm conditions), and these can only be obtained from a high spatiotemporal resolution survey designed for that purpose.

Acknowledgments

We greatly acknowledge SHN and INIDEP from Argentina for collecting and providing a vast majority of the in situ observations in the region, available from *Charo and Piola* [2014], from the World Ocean Database at the National Oceanographic Data Center (NODC, https://www.nodc.noaa.gov/OC5/WOD/pr_wod.html), and at http://www.inidep.edu.ar/oceanografia; Chris Linder for facilitating the MATLAB code to compute cross-front mean transects (available at http://www.whoi.edu/science/PO/people/clinder/software.html; James Pringle for useful discussions and two anonymous reviewers whose comments contributed to improve this manuscript; and Mati Kahru for processing and providing the satellite Chl-a data. NASA's Research, Education and Applications Solution Network (REASoN) and MEaSURES programs funded development of the CCMP wind fields, which are distributed by the Physical Oceanography Distributed Active Archive Center (http://podaac.jpl.nasa.gov/). MMC and STG were funded by a NASA NESFF fellowship (NNX12AN41H 001), NASA's Ocean Vector Wind Science Team (NASA NNX14A078G), and the Southern Ocean Carbon and Climate Observations and Modeling (SOCCOM) Project (NSF PLR-1425989). ARP acknowledges the support of grant CRN3070 from the Inter-American Institute for Global Change Research, which is supported by the US National Science Foundation grant GEO-1128040. SIR acknowledges the support of grant PIDDEF 47/12 from the Argentine Ministry of Defense.

References

Acha, E., H. Mianzan, R. Guerrero, M. Favero, and J. Bava (2004), Marine fronts at the continental shelves of austral South America: Physical and ecological processes, *J. Mar. Syst.*, *44*(1–2), 83–105.

Aikman, F., H. W. Ou, and R. W. Houghton (1988), Current variability across the New-England continental shelf-break and slope, *Cont. Shelf Res.*, *8*(5–7), 625–651.

Arruda, R., P. H. R. Calil, A. A. Bianchi, S. C. Doney, N. Gruber, I. Lima, and G. Turi (2015), Air-sea CO_2 fluxes and the controls on ocean surface pCO_2 seasonal variability in the coastal and open-ocean southwestern Atlantic Ocean: A modeling study, *Biogeosciences*, *12*(19), 5793–5809.

Artana, C., R. Ferrari, Z. Koenig, M. Saraceno, A. R. Piola, and C. Provost (2016), Malvinas Current variability from Argo floats and satellite altimetry, *J. Geophys. Res.: Oceans*, *121*, 4854–4872, doi:10.1002/2016JC011889.

Atlas, R., R. N. Hoffman, J. Ardizzone, S. M. Leidner, J. C. Jusem, D. K. Smith, and D. Gombos (2011), A cross-calibrated, multiplatform ocean surface wind velocity product for meteorological and oceanographic applications, *Bull. Am. Meteorol. Soc.*, *92*(2), 157–174, doi:10.1175/2010BAMS2946.2.

Bianchi, A. A. (2005), Vertical stratification and air-sea CO_2 fluxes in the Patagonian shelf, *J. Geophys. Res.*, *110*, C07003, doi:10.1029/2004JC002488.

Bianchi, A. A., D. R. Pino, H. G. I. Perlender, A. P. Osiroff, V. Segura, V. Lutz, M. L. Clara, C. F. Balestrini, and A. R. Piola (2009), Annual balance and seasonal variability of sea-air CO_2 fluxes in the Patagonia Sea: Their relationship with fronts and chlorophyll distribution, *J. Geophys. Res.*, *114*, C03018, doi:10.1029/2008JC004854.

Bisbal, G. A. (1995), The Southeast South American shelf large marine ecosystem: Evolution and components, *Mar. Policy*, *19*(1), 21–38.

Bogazzi, E., A. Baldoni, A. Rivas, P. Martos, R. Reta, J. L. Orensanz, M. Lasta, P. Dell'Arciprete, and F. Werner (2005), Spatial correspondence between areas of concentration of Patagonian scallop (*Zygochlamys patagonica*) and frontal systems in the southwestern Atlantic, *Fish. Oceanogr.*, *14*(5), 359–376.

Bourassa, M. A., E. Rodriguez, and R. Gaston (2010), NASA's ocean vector winds science team workshops, *Bull. Am. Meteorol. Soc.*, *91*(7), 925–928.

Bretherton, C. S., M. Widmann, V. P. Dymnikov, J. M. Wallace, Blade, and Ileana (1999), The effective number of spatial degrees of freedom of a time-varying field, *J. Clim.*, *12*, 1990–2009.

Brink, K. H. (2016), Cross-shelf exchange, *Annu. Rev. Mar. Sci.*, *8*(1), 59–78.

Campagna, C., A. R. Piola, M. Rosa Marin, M. Lewis, and T. Fernández (2006), Southern elephant seal trajectories, fronts and eddies in the Brazil/Malvinas Confluence, *Deep Sea Res., Part I*, *53*(12), 1907–1924, doi:10.1016/j.dsr.2006.08.015.

Carr, M. E., and E. J. Kearns (2003), Production regimes in four Eastern Boundary Current systems, *Deep Sea Res., Part II*, *50*(22–26), 3199–3221.

Carranza, M. M., and S. T. Gille (2015), Southern Ocean wind-driven entrainment enhances satellite chlorophyll-a through the summer, *J. Geophys. Res.*, *120*, 304–323, doi:10.1002/2014JC010203.

Carreto, J. I., V. A. Lutz, M. O. Carignan, A. Colleoni, and S. G. De Marco (1995), Hydrography and chlorophyll-a in a transect from the coast to the shelf-break in the Argentinian Sea, *Cont. Shelf Res.*, *15*(2–3), 315–336.

Carreto, J. I., N. G. Montoya, M. O. Carignan, R. Akselman, E. M. Acha, and C. Derisio (2016), Environmental and biological factors controlling the spring phytoplankton bloom at the Patagonian shelf-break front—Degraded fucoxanthin pigments and the importance of microzooplankton grazing, *Prog. Oceanogr.*, *146*, 1–21, doi:10.1016/j.pocean.2016.05.002.

Chapman, D. C. (2002), Sensitivity of a model shelfbreak front to the parameterization of vertical mixing, *J. Phys. Oceanogr.*, *32*, 3291–3298.

Chapman, D. C., and S. J. Lentz (1994), Trapping of a coastal density front by the bottom boundary layer, *J. Phys. Oceanogr.*, *24*(7), 1464–1479.

Charo, M., and A. Piola (2014), Hydrographic data from the GEF Patagonia cruises, *Earth Syst. Sci. Data*, *6*, 265–271, doi:10.5194/essd-6-265-2014.

Chavez, F. P., and M. Messié (2009), A comparison of Eastern Boundary Upwelling Ecosystems, *Prog. Oceanogr.*, *83*, 80–96, doi:10.1016/j.pocean.2009.07.032.

Chelton, D. B. (2004), Satellite measurements reveal persistent small-scale features in ocean winds, *Science*, *303*(5660), 978–983.

Combes, V., and R. P. Matano (2014), A two-way nested simulation of the oceanic circulation in the Southwestern Atlantic, *J. Geophys. Res. Oceans*, *119*, 731–756, doi:10.1002/2013JC009498.

Davis, R. E. (1977), Techniques for statistical analysis and prediction of geophysical fluid systems, *Geophys. Astrophys. Fluid Dyn.*, *8*(1), 245–277.
de Boyer Montégut, C., G. Madec, A. S. Fischer, A. Lazar, and D. Iudicone (2004), Mixed layer depth over the global ocean: An examination of profile data and a profile-based climatology, *J. Geophys. Res.*, *109*, C12003, doi:10.1029/2004JC002378.
Eichler, T. P., and J. Gottschalck (2013), A comparison of southern hemisphere cyclone track climatology and interannual variability in coarse-gridded reanalysis datasets, *Adv. Meteorol.*, *2013*(19), 1–16.
Falabella, V. (2009), *Atlas del Mar Patagónico. Especies y Espacios*, edited by V Falabella, C. Campagnay, and J. Croxall, Wildlife Conserv. Soc. and BirdLife Int., Buenos Aires.
Franco, B. C., A. R. Piola, A. L. Rivas, A. Baldoni, and J. P. Pisoni (2008), Multiple thermal fronts near the Patagonian shelf break, *Geophys. Res. Lett.*, *35*, L02607, doi:10.1029/2007GL032066.
Franks, P. J. S. (1992), Phytoplankton blooms at fronts: Patterns, scales and physical forcing mechanisms, *Rev. Aquat. Sci.*, *6*(2), 121–137.
Franks, P. J. S., and L. J. Walstad (1997), Phytoplankton patches at fronts: A model of formation and response to wind events, *J. Mar. Res.*, *55*(1), 1–29.
Fratantoni, P. S., and R. S. Pickart (2003), Variability of the shelf break jet in the Middle Atlantic Bight: Internally or externally forced?, *J. Geophys. Res.*, *108*(C5), 3166, doi:10.1029/2002JC001326.
Garcia, V. M. T., C. A. E. Garcia, M. M. Mata, R. C. Pollery, A. R. Piola, S. R. Signorini, C. R. Mcclain, and M. D. Iglesias-Rodriguez (2008), Environmental factors controlling the phytoplankton blooms at the Patagonia shelf-break in spring, *Deep Sea Res., Part I*, *55*(9), 1150–1166.
Gawarkiewicz, G., and D. C. Chapman (1992), The role of stratification in the formation and maintenance of shelf-break fronts, *J. Phys. Oceanogr.*, *22*, 753–773.
Gómez, M. I., A. Piola, G. Kattner, and V. A. Alder (2011), Biomass of autotrophic dinoflagellates under weak vertical stratification and contrasting chlorophyll levels in subantarctic shelf waters, *J. Plankton Res.*, *33*(8), 1304–1310.
Goni, G. J., F. Bringas, and P. N. Dinezio (2011), Observed low frequency variability of the Brazil Current front, *J. Geophys. Res.*, *116*, C10037, doi:10.1029/2011JC007198.
Guerrero, R. A., and A. R. Piola (1997), Masas de agua en la plataforma continental, *El Mar Argentino y sus Recursos Pesqueros*, *1*, 107–118.
Guerrero, R. A., A. R. Piola, H. Fenco, R. P. Matano, V. Combes, Y. Chao, C. James, E. D. Palma, M. Saraceno, and P. T. Strub (2014), The salinity signature of the cross-shelf exchanges in the Southwestern Atlantic Ocean: Satellite observations, *J. Geophys. Res. Oceans*, *119*, 7794–7810, doi:10.1002/2014JC010113.
Hales, B., R. D. Vaillancourt, L. Prieto, J. Marra, R. Houghton, and D. Hebert (2009), *J. Mar. Syst.*, *78*(3), 426–441.
He, R., K. Chen, K. Fennel, G. G. Gawarkiewicz, and D. J. McGillicuddy Jr. (2011), Seasonal and interannual variability of physical and biological dynamics at the shelfbreak front of the Middle Atlantic Bight: Nutrient supply mechanisms, *Biogeosciences*, *8*(10), 2935–2946.
Heileman, S. (2009), Patagonian shelf: LME, in *The UNEP Large Marine Ecosystem Report: A Perspective on Changing Conditions in LMEs of the World's Regional Seas*., edited by K. Sherman, and G. Hempel, UNEP Regional Seas Report and Studies, vol. 182, pp. 735–746, UNEP, Nairobi, Kenya.
Houghton, R. W., F. Aikman, and H. W. Ou (1988), Shelf-slope frontal structure and cross-shelf exchange at the New-England shelf-break, *Cont. Shelf Res.*, *8*(5–7), 687–710.
Hutchinson, D. K., A. M. C. Hogg, and J. R. Blundell (2010), Southern ocean response to relative velocity wind stress forcing, *J. Phys. Oceanogr.*, *40*(2), 326–339.
IOCCG (2004), Guide to the creation and use of ocean-colour, Level-3, binned data products, in *Reports of the International Ocean Colour Coordinating Group*, vol. 4, Dartmouth, Canada.
Jones, D. A., and I. Simmonds (1993), A climatology of southern-hemisphere extratropical cyclones, *Clim. Dyn.*, *9*(3), 131–145.
Kelly, K. A., S. Dickinson, M. J. McPhaden, and G. C. Johnson (2001), Ocean currents evident in satellite wind data, *Geophys. Res. Lett.*, *28*(1), 2469–2472.
Klein, P., and B. Coste (1984), Effects of wind-stress variability on nutrient transport into the mixed layer, *Deep Sea Res., Part A*, *31*(1), 21–37.
Klein, P., and B. Hua (1988), Mesoscale heterogeneity of the wind-driven mixed layer: Influence of a quasigeostrophic flow, *J. Mar. Res.*, *46*, 495–525.
Lee, D.-K., P. Niiler, A. Warn-Varnas, and S. Piacsek (1994), Wind-driven secondary circulation in ocean mesoscale, *J. Mar. Res.*, *52*, 371–396.
Le Traon, P. Y. (1990), A method for optimal analysis of fields with spatially variable mean, *J. Geophys. Res.*, *95*, 13,543–13,547.
Linder, C. A., G. G. Gawarkiewicz, and R. S. Pickart (2004), Seasonal characteristics of bottom boundary layer detachment at the shelfbreak front in the Middle Atlantic Bight, *J. Geophys. Res.*, *109*, C03049, doi:10.1029/2003JC002032.
Longhurst, A. (2007), The Atlantic Ocean, in *Ecological Geography of the sea*, 2nd ed., pp. 131–268, Elsevier, New York.
Lutz, V. A., V. Segura, A. I. Dogliotti, D. A. Gagliardini, A. A. Bianchi, and C. F. Balestrini (2010), Primary production in the Argentine Sea during spring estimated by field and satellite models, *J. Plankton Res.*, *32*(2), 181–195.
Machado, I., M. Barreiro, and D. Calliari (2013), Variability of chlorophyll-a in the Southwestern Atlantic from satellite images seasonal cycle and ENSO influences, *Cont. Shelf Res.*, *53*(C), 102–109, doi:10.1016/j.csr.2012.11.014.
Matano, R. P., and E. D. Palma (2008), On the upwelling of downwelling currents, *J. Phys. Oceanogr.*, *38*, 2482–2500, doi:10.1175/2008JPO3783.1.
Matano, R. P., V. Combes, A. R. Piola, R. Guerrero, E. D. Palma, P. Ted Strub, C. James, H. Fenco, Y. Chao, and M. Saraceno (2014), The salinity signature of the cross-shelf exchanges in the Southwestern Atlantic Ocean: Numerical simulations, *J. Geophys. Res. Oceans*, *119*, 7949–7968, doi:10.1002/2014JC010116.
McDougall, T. J., and P. M. Barker (2011), Getting started with TEOS-10 and the Gibbs seawater (GSW) oceanographic toolbox, *SCOR/IAPSO WG127*, pp. 1–34. [Available at www.TEOS-10.org.]
McGillicuddy, D. J., Jr. (2016), Mechanisms of physical-biological-biogeochemical interaction at the oceanic mesoscale, *Annu. Rev. Mar. Sci.*, *8*(1), 125–159.
Miller, R. N., R. P. Matano, and E. D. Palma (2011), Shelfbreak upwelling induced by alongshore currents: Analytical and numerical results, *J. Fluid Mech.*, *686*, 239–249, doi:10.1017/jfm.2011.326.
Mitchell, B. G., and M. Kahru (2009), Bio-optical algorithms for ADEOS-2 GLI, *J. Remote Sens. Soc. Jpn.*, *29*(1), 80–85.
Moffat, C., and S. Lentz (2012), On the response of a buoyant plume to downwelling-favorable wind stress, *J. Phys. Oceanogr.*, *42*(7), 1083–1098.
Morel, A., and J.-F. Berthon (1989), Surface pigments, algal biomass profiles, and potential production of the euphotic layer: Relationships reinvestigated in view of remote-sensing applications, *Limnol. Oceanogr*, *34*(8), 1545–1562.
Muller-Karger, F. E. (2005), The importance of continental margins in the global carbon cycle, *Geophys. Res. Lett.*, *32*, L01602, doi:10.1029/2004GL021346.

Nagai, T., A. Tandon, and D. L. Rudnick (2006), Two-dimensional ageostrophic secondary circulation at ocean fronts due to vertical mixing and large-scale deformation, *J. Geophys. Res.*, *111*, C09038, doi:10.1029/2005JC002964.
Nagai, T., A. Tandon, N. Gruber, and J. C. Mcwilliams (2008), Biological and physical impacts of ageostrophic frontal circulations driven by confluent flow and vertical mixing, *Dyn. Atmos. Oceans*, *45*(3–4), 229–251.
O'Reilly, J., S. Maritorena, B. Mitchell, D. Siegel, K. Carder, S. Garver, M. Kahru, and C. McClain (1998), Ocean color chlorophyll algorithms for SeaWiFS, *J. Geophys. Res.*, *103*(C11), 24,937–24,953.
Orsi, A., T. Whitworth, and W. Nowlin (1995), On the meridional extent and fronts of the Antarctic Circumpolar Current, *Deep Sea Res., Part I*, *42*(5), 641–673.
Painter, S. C., A. J. Poulton, J. T. Allen, R. Pidcock, and W. M. Balch (2010), The COPAS'08 expedition to the Patagonian Shelf: Physical and environmental conditions during the 2008 coccolithophore bloom, *Cont. Shelf Res.*, *30*(18), 1907–1923.
Palma, E. D., R. P. Matano, and A. R. Piola (2004), A numerical study of the Southwestern Atlantic Shelf circulation: Barotropic response to tidal and wind forcing, *J. Geophys. Res.*, *109*, C08014, doi:10.1029/2004JC002315.
Palma, E. D., R. P. Matano, and A. R. Piola (2008), A numerical study of the Southwestern Atlantic Shelf circulation: Stratified ocean response to local and offshore forcing, *J. Geophys. Res.*, *113*, C11010, doi:10.1029/2007JC004720.
Perez-Cenci, M., G. F. Caló, R. I. Silva, R. M. Negri, and G. L. Salerno (2014), The first molecular characterization of Picocyanobacteria from the Argentine Sea, *J. Mar. Biol.*, *2014*(1), 1–8.
Piola, A. R., and V. Falabella (2009), *El Mar Patagónico. Atlas del Mar Patagnico, Especies y Espacios*, edited by V. Falabella, C. Campagnay, and J. Croxall, pp. 55–75, Wildlife Conserv. Soc. of BirdLife Int., Buenos Aires.
Piola, A. R., E. J. D. Campos, O. O. Moller, M. Charo, and C. Martinez (2000), Subtropical Shelf Front off eastern South America, *J. Geophys. Res.*, *105*(C), 6565–6578.
Piola, A. R., S. I. Romero, and U. Zajaczkovski (2008), Space–time variability of the Plata plume inferred from ocean color, *Cont. Shelf Res.*, *28*(13), 1556–1567.
Piola, A. R., N. Martínez Avellaneda, R. A. Guerrero, F. P. Jardón, E. D. Palma, and S. I. Romero (2010), Malvinas-slope water intrusions on the northern Patagonia continental shelf, *Ocean Sci.*, *6*(1), 345–359.
Piola, A. R., B. C. Franco, E. D. Palma, and M. Saraceno (2013), Multiple jets in the Malvinas Current, *J. Geophys. Res. Oceans*, *118*, 2107–2117, doi:10.1002/jgrc.20170.
Podestá, G. P. (1990), Migratory pattern of Argentine hake Merluccius hubbsi and oceanic processes in the Southwestern Atlantic Ocean, *Fish. Bull.*, *88*(1), 167–177.
Poulton, A. J., S. C. Painter, J. R. Young, N. R. Bates, B. Bowler, D. Drapeau, E. Lyczsckowski, and W. M. Balch (2013), The 2008 Emiliania huxleyi bloom along the Patagonian Shelf: Ecology, biogeochemistry, and cellular calcification, *Global Biogeochem. Cycles*, *27*(4), 1023–1033.
Pyper, B. J., and R. M. Peterman (1998), Comparison of methods to account for autocorrelation in correlation analyses of fish data, *Can. J. Fish. Aquat. Sci.*, *55*(9), 2127–2140.
Ricker, W. E. (1973), Linear regressions in fishery research, *Fish. Rese. Board Can.*, *30*, 409–434.
Rivas, A. L. (2006), Quantitative estimation of the influence of surface thermal fronts over chlorophyll concentration at the Patagonian shelf, *J. Mar. Syst.*, *63*(3–4), 183–190, doi:10.1016/j.jmarsys.2006.07.002.
Romero, S. I., A. R. Piola, M. Charo, and C. A. E. Garcia (2006), Chlorophyll-a variability off Patagonia based on SeaWiFS data, *J. Geophys. Res.*, *111*, C05021, doi:10.1029/2005JC003244.
Saraceno, M., C. Provost, and A. R. Piola (2005), On the relationship between satellite-retrieved surface temperature fronts and chlorophyll-a in the western South Atlantic, *J. Geophys. Res.*, *110*, C11016, doi:10.1029/2004JC002736.
Schloss, I. R., G. A. Ferreyra, M. E. Ferrario, G. O. Almandoz, R. Codina, A. A. Bianchi, C. F. Balestrini, H. A. Ochoa, D. Ruiz Pino, and A. Poisson (2007), Role of plankton communities in sea-air variations in pCO_2 in the SW Atlantic Ocean, *Mar. Ecol. Prog. Ser.*, *332*, 93–106.
Segura, V., V. A. Lutz, A. Dogliotti, R. I. Silva, R. M. Negri, R. Akselman, and H. Benavides (2013), Phytoplankton types and primary production in the Argentine Sea, *Mar. Ecol. Prog. Ser.*, *491*, 15–31.
Siedlecki, S. A., D. E. Archer, and A. Mahadevan (2011), Nutrient exchange and ventilation of benthic gases across the continental shelf break, *J. Geophys. Res.*, *116*, C06023, doi:10.1029/2010JC006365.
Siedlecki, S. A., A. Mahadevan, and D. E. Archer (2012), Mechanism for export of sediment-derived iron in an upwelling regime, *Geophys. Res. Lett.*, *39*, L03601, doi:10.1029/2011GL050366.
Signorini, S. R., V. M. T. Garcia, A. R. Piola, C. A. E. Garcia, M. M. Mata, and C. R. Mcclain (2006), Seasonal and interannual variability of calcite in the vicinity of the Patagonian shelf break (38°S–52°S), *Geophys. Res. Lett.*, *33*, L16610, doi:10.1029/2006GL026592.
Signorini, S. R., V. M. Garcia, A. R. Piola, H. Evangelista, C. R. Mcclain, C. A. Garcia, and M. M. Mata (2009), Further studies on the physical and biogeochemical causes for large interannual changes in the Patagonian Shelf spring-summer phytoplankton bloom biomass, *NASA Tech. Memo.*, Goddard Space Flight Center Greenbelt, Md.
Song, H., J. Marshall, M. J. Follows, S. Dutkiewicz, and G. Forget (2016), Source waters for the highly productive Patagonian shelf in the southwestern Atlantic, *J. Mar. Syst.*, *158*, 120–128, doi:10.1016/j.jmarsys.2016.02.009.
Swart, S., S. J. Thomalla, and P. M. S. Monteiro (2015), The seasonal cycle of mixed layer dynamics and phytoplankton biomass in the Sub-Antarctic Zone: A high-resolution glider experiment, *J. Mar. Syst.*, *147*, 103–115, doi:10.1016/j.jmarsys.2014.06.002.
Thomas, L., and R. Ferrari (2008), Friction, frontogenesis, and the stratification of the surface mixed layer, *J. Phys. Oceanogr.*, *38*(11), 2501–2518, doi:10.1175/2008JPO3797.1.
Thomas, L. N., and C. M. Lee (2005), Intensification of ocean fronts by down-front winds, *J. Phys. Oceanogr.*, *35*(6), 1086–1102.
Thompson, L. (2000), Ekman layers and two-dimensional frontogenesis in the upper ocean, *J. Geophys. Res.*, *105*(C3), 6437–6451, doi:10.1029/1999JC900336.
Valla, D., and A. R. Piola (2015), Evidence of upwelling events at the northern Patagonian shelf break, *J. Geophys. Res. Oceans*, *120*, 7635–7656, doi:10.1002/2015JC011002.
Vera, C. (2003), Interannual and interdecadal variability of atmospheric synoptic-scale activity in the Southern Hemisphere, *J. Geophys. Res.*, *108*, 8077, doi:10.1029/2000JC000406.
Vivier, F., and C. Provost (1999), Direct velocity measurements in the Malvinas Current, *J. Geophys. Res.*, *104*(C9), 21,083–21,103.
Vivier, F., C. Provost, and M. P. Meredith (2001), Remote and local forcing in the Brazil–Malvinas region, *J. Phys. Oceanogr.*, *31*, 892–913, doi:10.1175/1520-0485(2001)031<0892:RALFIT>2.0.CO;2
Whitt, D. B., M. Levy, and J. R. Taylor (2017), Low- and high- frequency oscillatory winds synergistically enhance nutrient entrainment and phytoplankton at fronts, *J. Geophys. Res.*, *122*, doi:10.1002/2016JC012400.

Zhang, W. G., G. G. Gawarkiewicz, D. J. McGillicuddy Jr., and J. L. Wilkin (2011), Climatological mean circulation at the New England shelf break, *J. Phys. Oceanogr.*, *41*(10), 1874–1893, doi:10.1175/2011JPO4604.1.

Zhang, W. G., D. J. McGillicuddy Jr., and G. G. Gawarkiewicz (2013), Is biological productivity enhanced at the New England shelfbreak front?, *J. Geophys. Res. Oceans*, *118*, 517–535, doi:10.1002/jgrc.20068.

Zhang, Z., R. Hetland, and X. Zhang (2014), Wind-modulated buoyancy circulation over the Texas-Louisiana shelf, *J. Geophys. Res. Oceans*, *119*, 5705–5723, doi:10.1002/2013JC009763.